

Deterministic Lateral Displacement for Cell Sorting

Licentiate Thesis
Trung S. H. Tran



LUND
UNIVERSITY

Division of Solid State Physics and Nano Lund
Department of Physics
Lund University, Sweden
November, 2017

Contents

Abstract	ii
Preface and Acknowledgements	iii
Appended manuscripts	iii
List of Abbreviations.....	iv
List of Figures.....	v
1. INTRODUCTION	1
1.1 Thesis Objectives	1
1.2 Thesis Outline	2
2. DETERMINISTIC LATERAL DISPLACEMENT	3
2.1 Microfluidics and Lab-on-a-Chip	3
2.2 DLD Theory and Factors Influences	4
2.3 State of the Art	7
3. OPEN CHANNEL DLD AND PAPER FLUIDICS.....	8
3.1 Open Microfluidics	8
3.2 Open Channel DLD.....	9
3.3 Capillary Paper Pump	10
3.4 Open DLD for Particles and Cell Sorting	11
4. DEFORMABILITY-BASED SEPARATION.....	14
4.1 Deformability Marker	14
4.2 Deformability and Cell Sorting	15
5. METHODS AND EXPERIMENTS	18
5.1 Device Fabrication and Sample Preparation	18
5.2 Image acquisition and analysis.....	19
5.3 Experiment Setup	20
6. SIGNIFICANCE STATEMENT OF MANUSCRIPTS	21
6.1 Open DLD Channel for Particles and Cell Sorting	21
6.2 Sorting Breast Cancer Cells Based on Deformability.....	22
7. CONCLUSIONS AND OUTLOOKS	23
Appendix.....	24
Bibliography.....	26

Abstract

In the fields of medicine and biology, the separation of particles is a necessary step in many preparative and analytical processes. Deterministic lateral displacement has been a promising technique in the field of particle and cell sorting, especially for label-free separation. Applications of deterministic sorting by size, shape, and deformation have been reported in the literature over the last decade. However, the conventional use of pressure pumps, electrical actuation or syringe pumps, alone or parallel, requires complicated equipment, setups, and operations. With those requirements these devices are difficult to transport, need trained personnel and are associated with high running costs. In fact, they are often not fully compatible with point-of-care applications, especially in resource-poor setting. The first part of this Licentiate thesis focuses on an alternative way to handle and operate a microfluidic DLD device for a sorting application, which is portable and user friendly for the end-users. A combination of PDMS-based DLD and a paper-based pump is a key component of this approach. Several sorting applications towards biological samples such as blood fractionation, trypanosome enrichment, and breast cancer cell extraction are performed efficiently in terms of potential purity and capture rate. Moreover, the advantages of our open surface platform with regards to cleaning, reusing and integration are carefully addressed as well. Despite those benefits, this approach is still limited in terms of well-controlled flow-rate, which is the main requirement of our second study in deformability-based separation. Thus, by precisely controlling the flow in a microfluidic channel, we can carefully control the shear, which causes the deformation of soft particles and as a result, adjusts those particles' behavior in the DLD array. Separation of cancer cells from a heterogeneous sample is known as a challenging task due to the similarity among the physical properties of the cells, such as size, shape and surface charge. Furthermore, deformability has been reported as a potential parameter for cell isolation where a specific molecular marker is lacking. We show proof of principle of deformability-based DLD for isolating breast cancer cells (MCF7) from human breast cells (MCF10A).

Preface and Acknowledgements

First of all, I would like to thank Prof. Jonas Tegenfeldt and Dr. Jason Beech for their support during my projects. Their knowledge and deep insight into the physics and specifically in Deterministic Lateral Displacement technique are very valuable and encouraged me a lot. Thanks also to Stefan Holm and Bao Ho for microfabrication and support in the lab.

I like to thank my group mates for a lot of nice discussions and experienced comments. And I also thank the whole Bio-group at the Solid State Physics Department at Lund University, Faculty of Engineering. The vibrant atmosphere and interesting discussions in this group were a true pleasure to experience.

Last but not least, special thanks are due to my parents and family.

This work was carried out within NanoLund at Lund University with funding from the Child Cancer Foundation (MT2013-0031), LAPASO (EU FP7 project 607350) and the Swedish Research Council (VR) grant no. 2015-05426.

Appended manuscripts

The following research papers are included in this thesis:

I. Open channel deterministic lateral displacement for particle and cell sorting

Tran, Trung S.H., Ho, Bao D., Beech, Jason P., Tegenfeldt, Jonas O.,
Lab on a Chip, 2017. [DOI: 10.1039/C7LC00707H]

I did all experiments, analyzed the data. B. Ho contributed to the parts of Electrode experiment and paper measurements. J. Beech performed confocal microscopy and macro photography. I wrote the manuscript together with J. Beech.

II. Sorting Breast Cancer Cells Based on Deformability (manuscript)

Trung S.H. Tran, Jason P. Beech and Jonas O. Tegenfeldt.

I did all experiments, analyzed the data and wrote the manuscript.

List of Abbreviations

BSA	Bovine serum albumin
DI water	Deionized water
DLD	Deterministic Lateral Displacement
G	DLD gap distance
MCF7	Michigan Cancer Foundation-7 (breast cancer cell line)
MCF10A	Michigan Cancer Foundation-10A (human breast cell line)
LOC	Lab-On-a-Chip
PDMS	Poly-Di-Methyl-Siloxane
PLL-(g)-PEG	Poly (L-Lysine)-graft-Polyethyleneglycol
POC	Point-of-care
RBCs	Red Blood Cells
R_c	Critical Radius
WBCs	White Blood Cells
GFP	Green Fluorescent Protein

List of Figures

Figure 2-1 Microfluidics in the relationship to other fields.....	3
Figure 2-2 Various microfluidic sorting techniques.....	4
Figure 2-3 Size-based separation of particles on a pillar array	5
Figure 2-4 Overview of DLD parameters.	6
Figure 2-5 A typical sample of sorting capability in DLD	6
Figure 3-1 Main categories of open microfluidics.....	8
Figure 3-2 Original open channel DLD.....	9
Figure 3-3 A model of open channel DLD.....	10
Figure 3-4 Sample collection from paper fractions.....	11
Figure 3-5 Open DLD for particle sorting.....	12
Figure 3-6 Cell sorting in open DLD applications.....	12
Figure 3-7 Cleaning and reusing in open device.....	13
Figure 4-1 Different approaches for deforming a spherical particle.....	14
Figure 4-2 Normal and Cancer cell characteristic	15
Figure 4-3 Differences of rigid and soft particles in DLD array	16
Figure 4-4 Performance of individual cells in DLD array under different shear rates.....	16
Figure 4-5 Outlet distribution of two cell types as a function of pressure	17
Figure 5-1 Schematic overview of all experiments in this thesis	20
Figure 6-1 Graphical abstract for Open DLD technique	21
Figure 6-2 Schematic of deformability-based separation	22
Figure 7-1 Size and shape measurement	24
Figure 7-2 Comparison of different samples.....	24

Chapter 1

INTRODUCTION

1.1 Thesis Objectives

Microfluidics has greatly contributed to biotechnology and has been improving quickly in the last decade. By precisely controlling fluids and rapidly processing samples, it has become a potentially attractive alternative to some traditional experimental methods (1). A promising aspect of microfluidics is the classification of biological particles from heterogeneous samples. Indeed, microfluidic separation techniques have the ability to separate particles with high precision and resolution in terms of a variety of physical properties and principles (2). These sorting technologies are identified as either active methods that apply external forces to sort particles or passive methods that use inertial forces, obstacle arrays, and other mechanisms to achieve the separation.

One of the more promising sorting techniques, which provides a high resolution and throughput, is deterministic lateral displacement (DLD). DLD is a passive sorting method, which has a wide range of potential applications from nanoscale (DNA, exosomes) to microscale (blood, cells) or even large particles (fungal spores). It is based on various physical properties for sorting (size, morphology, surface charge, and deformation, etc.) (3).

In this Licentiate thesis, DLD is the main technique, which is described and repeatedly applied in different contexts in each chapter. Polymeric particles in a wide range of sizes and stiffness were used as a reference to confirm the sorting capability of DLD devices. Biological samples (blood, trypanosome, cell and cancer cell lines) were then targeted for sorting. Overall, two main objectives will be addressed in this work

- The first objective is to propose a simple microfluidic tool, which is easy to handle, equipment-free and capable of sorting typical samples.
- The second objective is to achieve softness sorting with the goal of cancer cell isolation. Here MCF7 and MCF10A are used as a model system for normal and cancerous cells.

Following is an introduction to the subject matter of this Licentiate thesis.

1.2 Thesis Outline

After this Introduction chapter, the thesis gives a brief description of microfluidics and microfluidic sorting techniques, specifically focusing on Deterministic Lateral Displacement, in **Chapter 2**. **Chapter 3** introduces an open DLD and paper capillary pump to achieve a simple and portable DLD chip. Cell deformability is presented in **Chapter 4**. The chapter focuses on cancer cell deformability and what factors influence it and the deformation-based DLD method. **Chapter 5** describes methods and practical details of each experiment. The significance of each manuscript is presented in **Chapter 6**. An outlook for remaining and future works is discussed in **Chapter 7**. Finally, **one published research paper and one manuscript** along with their electronic supplement information as well as appendix are found at the end of the thesis.

Chapter 2

DETERMINISTIC LATERAL DISPLACEMENT

2.1 Microfluidics and Lab-on-a-Chip

Microfluidics is a multi-disciplinary field encompassing engineering, physics, chemistry, biochemistry, nanotechnology, and biotechnology. By controlling and manipulating liquids at low volume (micro-nano scale), microfluidics has achieved many practical applications such as multiplexing, automation, and high-throughput screening. Lab-on-a-chip (LOC) technology is a concept in which several preparative or analytical processes are integrated onto a single chip that fits in a human hand. The improvement of LOC technology is intrinsically linked to microfluidics and micro-technology of semiconductors.

Microfluidics has been evolved extremely fast since the contribution of microelectronics in the mid-1950s. Using the photolithography technique in micro-fabrication, the first LOC of gas chromatography was created in 1979 (4). However, the field remained largely unexplored until the advent of soft lithography, which adapted microfabrication processes for use with polymer chips, was introduced in the late 80s (5). This solution opened the ability to easily fabricate polymer chips in any lab and offered a wide range of applications in materials, chemistry, and biology (Figure 2-1).

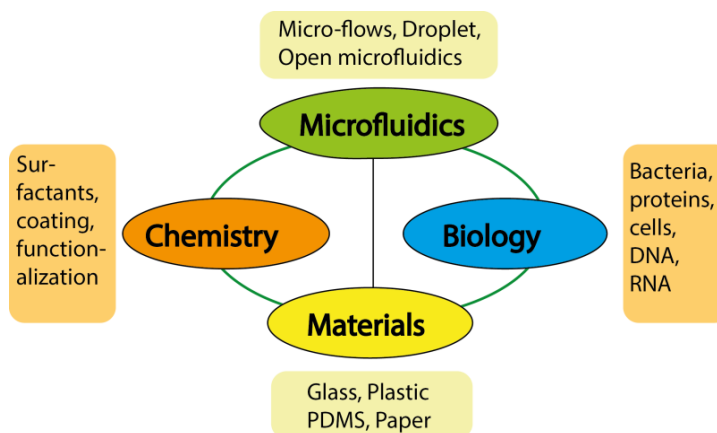


Figure 2-1 Microfluidics in the relationship to other fields

Microfluidics is mainly applied to biotechnology, which requires highly sophisticated tools with automated and efficient approaches. One of the greatest achievements is an amplification of DNA strands by massively parallel PCRs (polymerase chain reaction)(6, 7). Other different techniques were

succeeded for sequencing DNA, genomics, protein analysis and biorecognition. On the micro-scale, cell studies have been developed quickly for the pharmaceutical industry (8). Those include cell cultures, cellular communication, cell proliferation, migration and stem cell differentiation, cellular mechanics.

In preparation for such studies, there are many factors that need to be considered and solutions will depend strongly on the types of samples targeted and their specific properties. For instance, cells can be described by intracellular properties (DNA, RNA, and protein molecule interactions) or extracellular physical properties (size, morphology and surface protein expression). In fact, the need for isolation and sorting of cells according to different properties of interest is a central component. Researchers have already used a mix of flow-cytometry, magnetic separation, and density-gradient separation but newer, chip-based technologies, could greatly advance the field.

In the field of particle and cell sorting, microfluidics can offer accurate and high-throughput methods, which are comparable to conventional methods. Those can be classified as either active or passive sorting (Figure 2-2). An alternative way to categorize the field is fluorescent label-based sorting, bead-based sorting and label-free sorting (2).

While fluorescent label-based sorting relies on molecular interactions to selectively identify the types of cells, label-free separation is based on inherent physical characteristics of the cell. Such physical markers could be cell size, shape, deformability, density, electrical polarizability, electrical impedance, magnetic susceptibility and hydrodynamic properties (9).

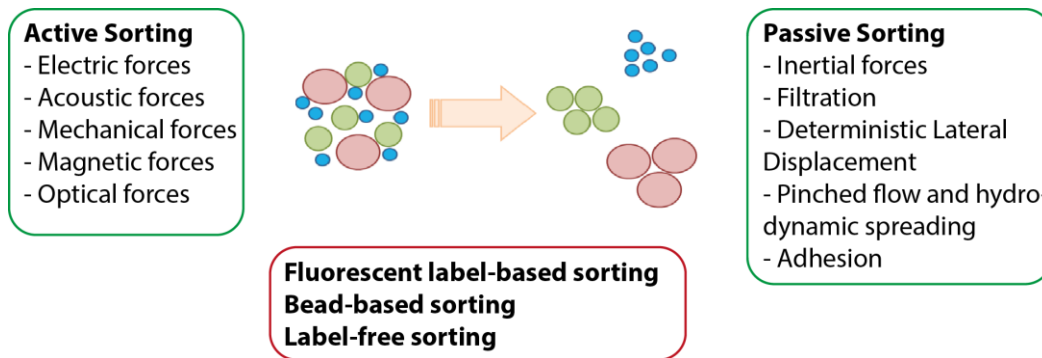


Figure 2-2 Various microfluidic sorting techniques

The work in this thesis is based on Deterministic Lateral Displacement, a passive and label-free sorting technique. More specifically, the two main topics focused on here are: easy-to-use open DLD for general sorting applications and, deformability-based DLD for cancer cells.

2.2 DLD Theory and Factors Influences

Deterministic Lateral Displacement (DLD) is a passive particle separation technique. It was first introduced in 2004 by Huang *et al.* and his colleagues for separation of microspheres and for DNA separation (10). For a simple explanation, the separation of particles occurs inside a pillar array as shown in Figure 2-3. The sample, consisting of a heterogeneous population, is loaded into an array of obstacles. Those particles pass through the pillar array in different paths depending on their sizes. Small particles move straight, following the flow while the big particles are displaced in relationship to the flow direction, and huge particles are trapped in the entrance of the array. The trajectory of each particle is a

function of its effective size. The effective size, in turn, is determined by a combination of size, shape and orientation of the particle in a certain position.

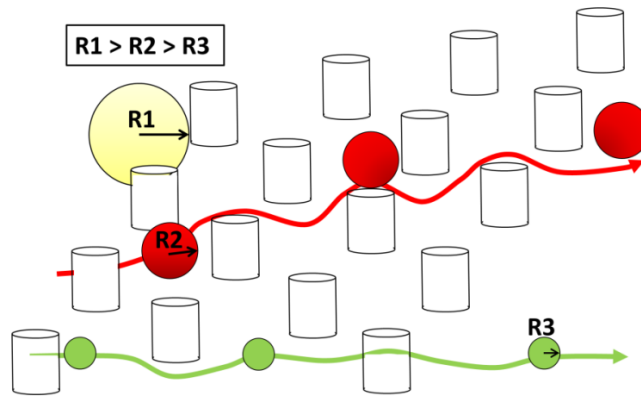


Figure 2-3 Size-based separation of particles on a pillar array

Before introducing DLD theory and the factors that influence particle behaviors, a brief review of fluid flow in microfluidics is necessary. In microfluidics, continuum fluid dynamics is described by the Navier-Stokes equation:

$$-\nabla p + \eta \nabla^2 \mathbf{u} = 0$$

where ∇p is the gradient of the pressure, η is the dynamic viscosity, u is the velocity of the fluid. This equation is simplified from Newton's second law when the inertial term is negligible, which is the case for very low Reynolds numbers ($Re \leq 10^{-3}$). The Reynolds number is the ratio between inertial and viscous effects. For a fluid with density ρ , viscosity η , average velocity u and characteristic dimension D , the Reynolds number is calculated using the following equation

$$Re = \frac{\rho u D}{\eta}$$

Due to the small channels in microfluidics (with a diameter ranging from 100nm to 100 μ m), the Reynolds number is small and usually less than 500 where the flow is completely laminar and no turbulence occurs, but the mass transfer Péclet number (competition between convection and diffusion) is often large.

In laminar flow (or streamline flow), the motion of particles is confined to streamlines. Thus, in a straight channel, particles move parallel to each other although their velocities can vary according to their positions. Furthermore, if a particle can be switched to another streamline when moving, it can be sorted out in the end from the initial mixture. Relying on the property of laminar flow, various methods apply an external force to push the targeted particles away from one streamline to another and consequently achieve separation (active sorting techniques).

As a passive sorting technique, DLD array also changes the streamlines of targeted particles, but it does this through interactions between the particles and the pillar array, and not through externally applied fields. The separation performance of each DLD device is based on its critical size (D_c). Davis *et al.* gave

an empirical formula describing the critical size based on experiments with a parabolic flow profile and rigid spherical particles (11):

$$D_C = 1.4GN^{-0.48}$$

where D_C is the critical diameter, G is the gap between two posts, and N is the period of the array. This equation can be expressed in some practical parameters as shown in Figure 2-4. Note that $N=\lambda/\Delta\lambda$.

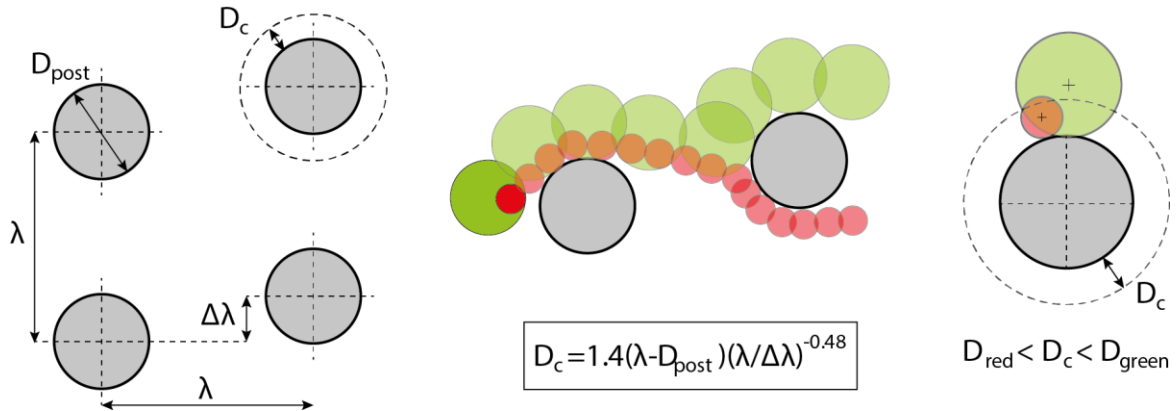


Figure 2-4 Overview of DLD parameters.

The critical size is an important parameter for the sorting characteristics of a DLD device. All particles smaller than a critical size move in zig-zag mode with the flow while bigger ones are displaced in relation to the flow direction. Gap size and the depth of a device are other device parameters that need to be considered carefully for particle sorting due to trapping or clogging. Particles bigger than device depth or gap size may be trapped in the reservoirs or in the entrance of array.

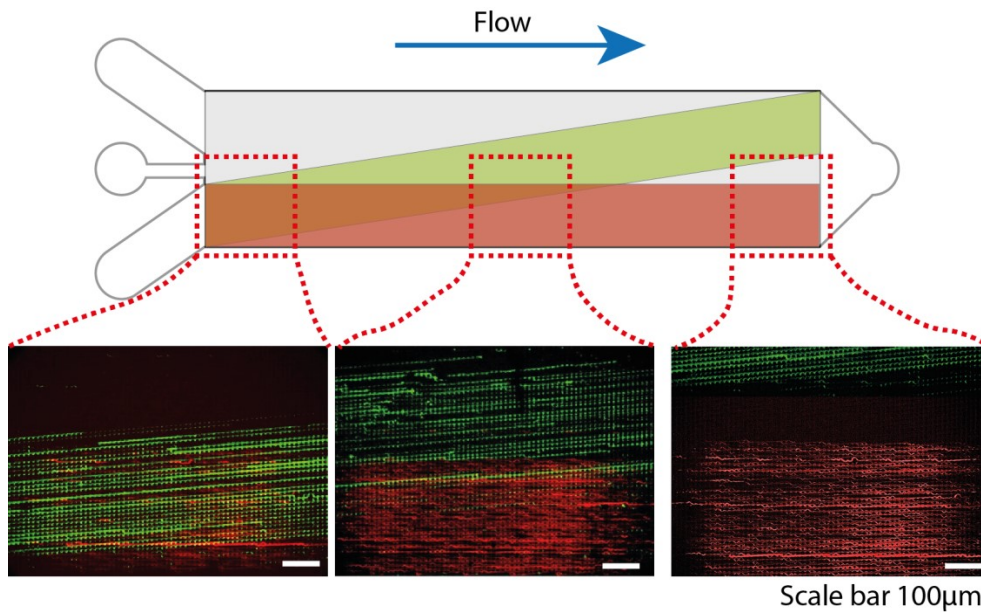


Figure 2-5 A typical sample of sorting capability in DLD

An overview of particle separation in a DLD device is shown in Figure 2-5. Here, a mixture of two fluorescent polystyrene beads (green 16 μ m and red 5 μ m) was introduced in an inlet of DLD device. The array was designed such that $D_c=10.5\mu$ m, gap size $G=23\mu$ m and depth is 24 μ m. The images were captured in different positions (near the inlet, in the middle of the device and near the outlet) and provide an overview of particle separation.

In general, when discussing the performance of sorting devices, the important parameters are purity, capture rate, resolution, and throughput. For biological samples or cells, cell viability, and cell recovery can be added to this list. Overall, the sorting efficiency is evaluated based on which combination of these parameters is most important in each separate case (high purity, high throughput or cell recovery, etc.). In the next chapter in this thesis, the different targets of sorting will be expressed clearly.

2.3 State of the Art

During the last decade, since the first applications for particle sorting and for DNA separation (10), the DLD technique has evolved dramatically and has been adapted to a variety of biological samples and sample properties. Plenty of effort has been made to understand deeply the theory as well as design considerations for new target samples. Examples of DLD applications are the fractionation of blood components (12-15), isolation of cancer cells from blood cells (16-18), parasite separation (19), isolation of extracellular vesicles (20-22).

Essentially, DLD is a size-based sorting technique. In 2011, Holm *et al.* has reported it as a morphology-based sorting tool in parasite extraction (19). DLD also has been evaluated as a deformability-based sorting in red blood cells (23) and platelets (24). These capabilities enable us to address a wide range of DLD applications.

When operating DLD, clogging due to particle-particle and particle-surface interactions is a practical challenge. Chemical surface treatment using PLL-PEG, BSA or Pluronic has been used to prevent this limitation but new solutions are still required for highly concentrated and sticky samples.

We believe that potentially, DLD could be used to perform sorting of irregularly shaped and/or deformable heterogeneous samples. Furthermore, DLD arrays can be designed and integrated with up and downstream processes to achieve a complete lab-on-a-chip system.

Chapter 3

OPEN CHANNEL DLD AND PAPER FLUIDICS

3.1 Open Microfluidics

The first microfluidics was introduced in closed or confined micro-flows. These microfluidic systems called Lab-on-a-Chip have many advantages, compared to standard beakers or test tubes. They use a small volume of sample and costly reagents and contribute to reduce operating times. These microfluidic devices most commonly require external systems to generate flows to the chip. Different types of pumps, valves, reservoirs, syringes have been developed to precisely manipulate microflows.

In order to create a portable chip without external equipment, capillary flow that moves the liquids automatically in the microchannel was introduced. The first studies of capillary flow were conducted in cylindrical tubes by Cameron, Bell, Lucas, Washburn, and Rideal in the 1910s (25, 26). With the development of trigger valves and capillary pumps, studies on capillary flows have seen a revival (27).

The open microfluidic system has the advantages of accessibility: addition of reagents, pipetting for the addition or retrieval of biologic liquids or objects, and human interventions on the system can then all be easily performed. Also, optical observation is facilitated. Finally, these systems have the ability to eliminate air bubbles and clogged devices can be more easily cleaned, two things that can be hard to do in closed systems. The limit of detection (LOD) and scalability are also being continuously improved in open systems. Overall, all these aspects contribute to making open microfluidics an interesting choice for point-of-care and home-care systems.

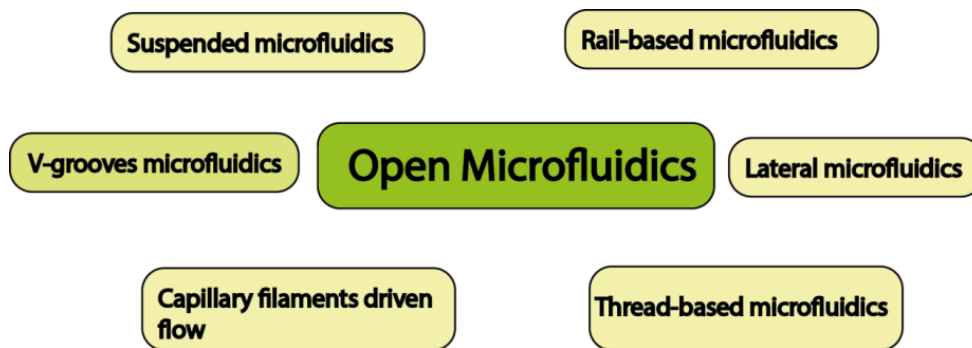


Figure 3-1 Main categories of open microfluidics

Open microfluidics can be divided into various subgroups: lateral microfluidics, suspended microfluidics, rail-based microfluidic, thread-based microfluidics, V-grooves microfluidics and capillary filaments driven flow (28) (Figure 3-1)

As a potential solution for a portable device, in this study we investigated the use of capillary flow in DLD systems. The following parts of this chapter present a model of open channel DLD and paper capillary pump, together with the physics of capillary flow and some examples of sorting applications.

3.2 Open Channel DLD

While standard DLD devices most commonly use confined fluids in closed channels, open channel DLD operated by capillary flow shows a promising alternative, Figure 3.2 (reproduced with permission from J.Beech and Tegenfeldt). It was introduced by J.Beech *et al.* at MicroTas 2009 (29).

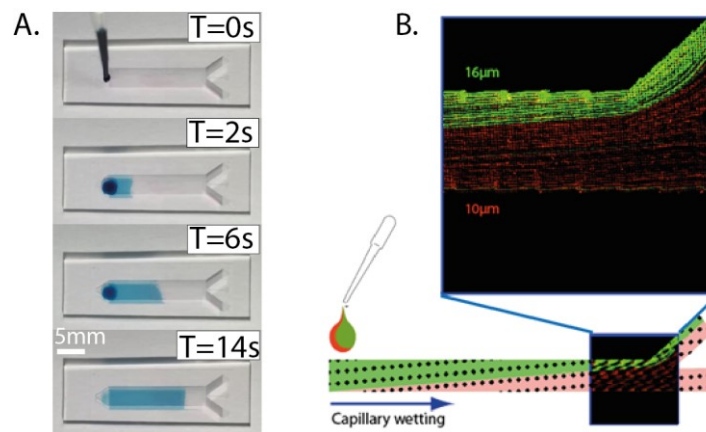


Figure 3-2 Original open channel DLD

By removing the lid of a DLD device and treating the surface with oxygen plasma, the authors created a capillary flow (Figure 3-2A) that dragged the particles through the DLD array fabricated in PDMS. Big particles (green $16\mu\text{m}$) larger than the critical size $D_c = 10\mu\text{m}$ were displaced in relation to the flow direction (Figure 3-2B). However, this method is limited by sample volume and collection as well as a requirement for oxygen plasma to treat the surface of PDMS (hydrophobic surface). Furthermore, the sorting result was limited in term of purity of fractions (one was small particles and another fraction was the mixture).

What we have done in the present work that is new is that we replaced the hydrophilic treatment, increased sample volumes, collected sorted fractions and enhanced the sorting purity as shown in Figure 3-3. We also used the approach to perform separations on several parameters other than just size. In detail, a traditional DLD device can sort the particles completely in different fractions with two inlets. Instead of using a single inlet as in the previous study, two inlet reservoirs give better control of the sample and allows for loading of a larger volume. Most importantly, it allows the sorted fraction to enter a clean buffer, thereby ensuring high purity. By immersion or pre-wetting of the PDMS in a water bath, the device is ready to use without oxygen plasma or other type of hydrophilic treatment. In addition, a paper which has two chambers separated by wax lines is used to collect all sorted fractions as well as to pull the liquid as a capillary pump.

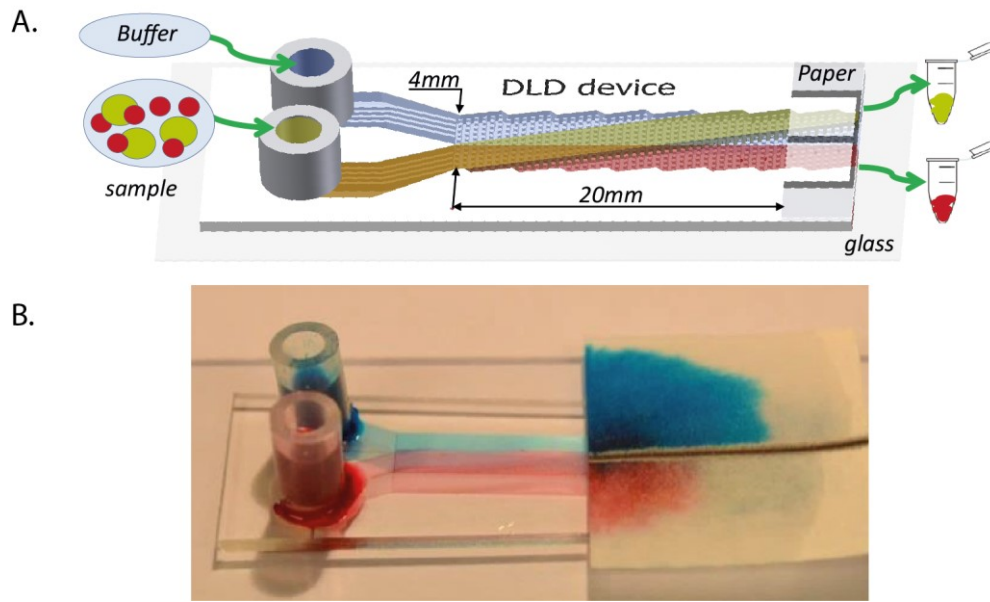


Figure 3-3 A model of open channel DLD

A complete model of open DLD device contains a PDMS stamp, two inlet reservoirs, and an additional paper pump with wax lines. For practical use, the sample and buffer are loaded separately in two inlets of a pre-wetted PDMS device. By the capillary flow and the sorting mechanism in the DLD array, the sample is sorted in different fractions and is collected by the paper. Figure 3-3A presents a whole process of sorting in an open DLD device. When the sorted fractions stay in the paper, a downstream analysis could be directly conducted or a process of particle extraction could easily be done in a vortex step. The function of the paper will be explained in the following section.

A characterization of the liquid profile along the device could be found in three experimental approaches: a macro photography image of the liquid inside the DLD array, a confocal image of 3D liquid volume and a study of the flow in the channel. The results give a better understanding of flow inside the open DLD channel and confirm that the fluid is confined in an open channel (more details can be found in the section of *DLD devices in open configuration* in Paper 1 “*Open channel DLD for particle and cell sorting*”). Overall, open channel DLD with new components (reservoirs and paper) are easy to assemble and easy-to-use with particular relevance to applications in resource-poor settings.

3.3 Capillary Paper Pump

As mentioned above, the paper plays an important role in an open DLD system. The paper provides a good solution to maintaining a continuous flow, which is important to achieve a continuous sorting. As a capillary pump, the paper contributes a negative pressure to increase and stabilize the flow rate. A study of the flow rate in the open channel DLD as well as in the paper with evaporation taken into account was conducted in different experiments. Compared to the flow driven by the capillary wetting of the paper, the flow due to the hydrostatic pressure of fluid in reservoirs and the absorption rate of paper are significantly less in magnitude. With a paper fluidics geometry that allows the sample to wet the paper in semicircle or half a semicircle the resulting flow is essentially constant.

Another aspect of paper, which is constructed by a fiber matrix, is that it is an attractive substrate for various biomedical applications. Paper based lateral flow tests without the need for specialized and costly equipment are used for medical diagnostics, POC tools and home-care testing. Furthermore, paper-based cell culturing has been developed as a promising approach that allows cells to grow in both 2D and 3D cultures. In this study, paper was used as a convenient substrate that is easy to collect, transport or release the sorted sample from in order to pass it to subsequent analysis. In practice, after sorting all needed particles in an open DLD, the paper is cut out into different fractions and the isolated particles are released into suspension by vortexing and spinning (Figure 3-4B,C).

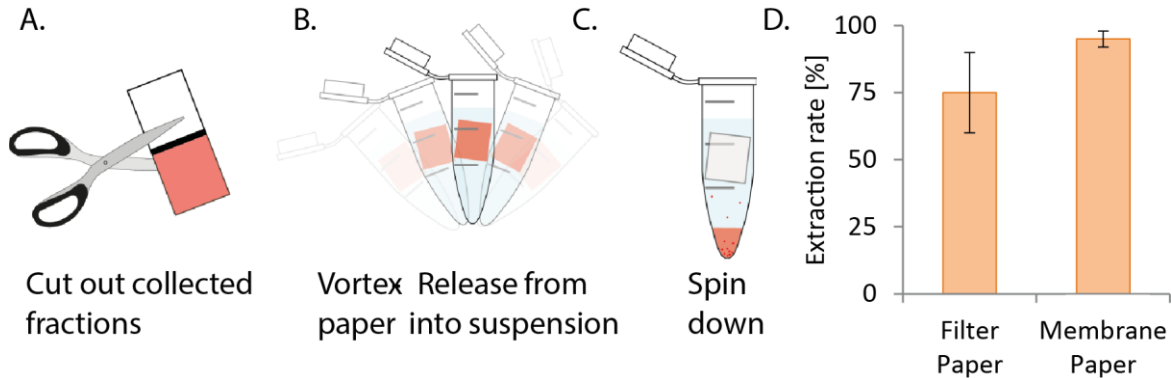


Figure 3-4 Sample collection from paper fractions

Various types of paper with different pore sizes, retentions and materials were tested in terms of absorption rate and sample extraction rate. Among these, a filter paper with a good absorption rate was selected for use as a capillary pump and a sandwich paper (filter paper and membrane paper) was applied to increase the sample extraction rate. A comparison of extraction rates is shown in Figure 3-4D. In future work, a bio-compatible paper for cell culture or lateral flow paper could be utilized in the open channel DLD substrate for integrating a series of POC tools.

3.4 Open DLD for Particles and Cell Sorting

A model of the open DLD and capillary paper pump is shown as an illustration of the continuous flow/sorting as well as the capability of sample collection. With flow driven by a paper capillary pump, this method exhibits the same sorting capability for particles and as conventional DLD.

Polystyrene beads, which range from $2\mu\text{m}$ to $20\mu\text{m}$ were used to characterize the sorting efficiency of open DLD devices. Three DLD designs with critical sizes of $5.1\mu\text{m}$, $10.7\mu\text{m}$ and $14.5\mu\text{m}$ were assembled, with reservoirs and a filter paper, and separations tested (Figure 3-5A). Fluorescent trajectories of $3\mu\text{m}$ and $7\mu\text{m}$ in device 1 gave an overview of sorting process in an open DLD system and in paper (Figure 3-5B). A summary of particle behavior in the three devices is plotted in terms of zig-zagging beads (black dots) and displaced beads (white dots). The critical size in each device was calculated by Davis' equation (11) and the experimental data confirmed that there is no significant difference between the critical sizes in open and closed devices (Figure 3-5C).

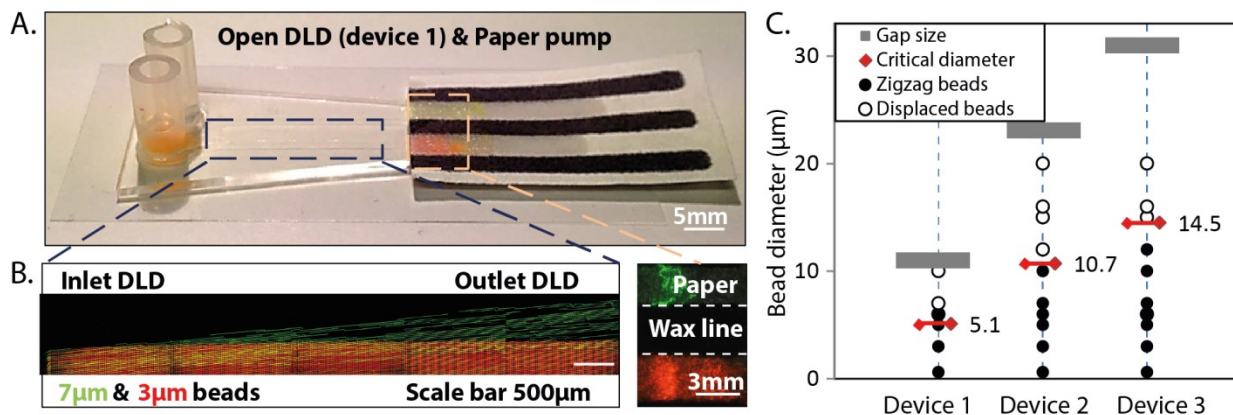


Figure 3-5 Open DLD for particle sorting

To test biological applications, we used the open DLD technique for a range of mixtures of samples in several different sorting schemes. As a powerful mechanism for size-based sorting, traditional DLD and open DLD perform similarly for blood fractionation (RBCs and WBCs) and cancer cell isolation (MCF7 and RBCs). Figure 3-6A presented a typical setup of sorting MCF7 from blood and trajectories of two kinds of cells were observed without fluorescence. The RBCs are prevalent at a higher concentration than the MCF7 cells so they can easily be visualized in the paper. To evaluate the purity of sorting, fluorescent dyes were added to both cells in a different experiment (Figure 7 in Paper 1).

Morphology-based sorting is another promising aspect of DLD applications. In this study, Trypanosomes were isolated and enriched from RBCs in an open DLD device with depth 9µm. In another example of open DLD we sorted single cells from clusters of MCF7 cells. A summary of the cell sorting in open DLD is found in Figure 3-6C.

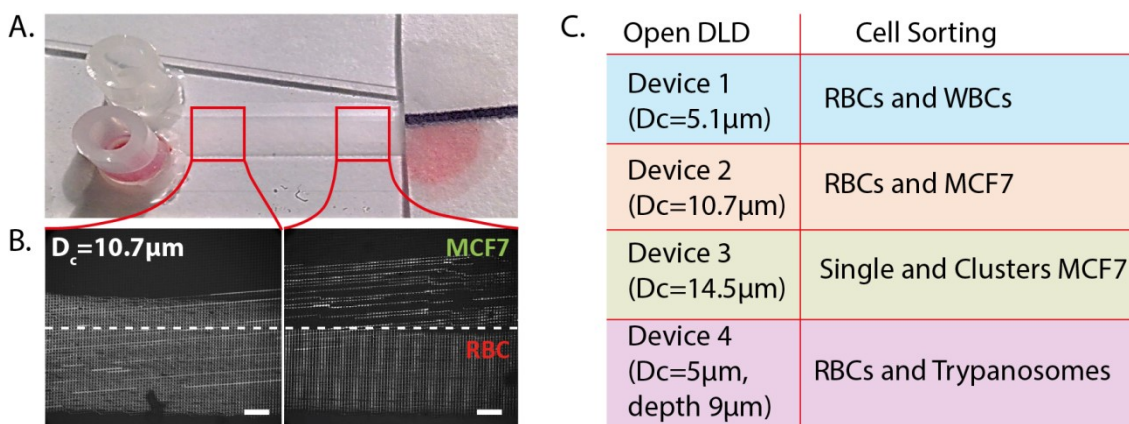


Figure 3-6 Cell sorting in open DLD applications

To measure the effect of sorting in open devices on cell health, cell viability assays and proliferation assays were conducted. High viability (>90%) and no significant difference in cell proliferation rate were observed for cells sorted in open devices. The performance of the open devices is comparable to the closed system with the same sorting efficiency. An additional advantage of open devices is the ease with which they can be cleaned and reused. A closed DLD device, which is sealed to prevent leaking, is hard to

clean and reuse when clogging happens (Figure 3-7A and B) while an open device can potentially be reused after a cleaning step (Figure 3-7C). Furthermore, a preliminary test with electrokinetics combined with DLD showed that electrodes are easily introduced into an open device.

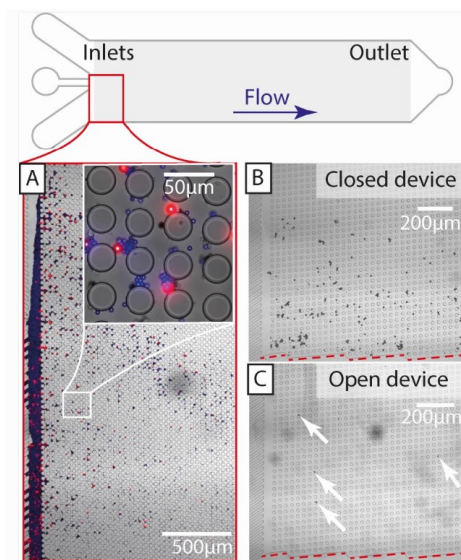


Figure 3-7 Cleaning and reusing in open device

Finally, we have successfully demonstrated that open channel DLD devices assembled with capillary paper pumps are promising portable tools for particle and cell sorting. In terms of size-based sorting and morphology-based sorting as well as potential to integrate with other technique, such as electrokinetics and paper fluidics, we have shown that open channel DLD has the potential to open up for new applications.

Chapter 4

DEFORMABILITY-BASED SEPARATION

4.1 Deformability Marker

The mechanical properties of single cells can be used as a biomarker to determine cell phenotypes, especially for diagnoses where molecular markers are lacking. Among these properties, cell size and cell morphology are two basic label-free markers, which are commonly used to discriminate between different cell types. In the microfluidics and sorting fields, these characteristics have been mainly exploited in a variety of techniques including active and passive methods. Size and morphology based sorting in DLD arrays was already described in the previous chapter. However, size and morphology are not always sufficient to identify cells, especially cancer cells. Cancer cells, which grow abnormally and can be transformed from normal cells may have the same size and shape as the original cell. Furthermore, cancer cells may have a wider size distribution than normal cells within a given cell type. In case of the morphology, irregular shapes were found in cancer cells more than in normal cells. The overlapping of these characteristics remains a challenge for cancer cell isolation.

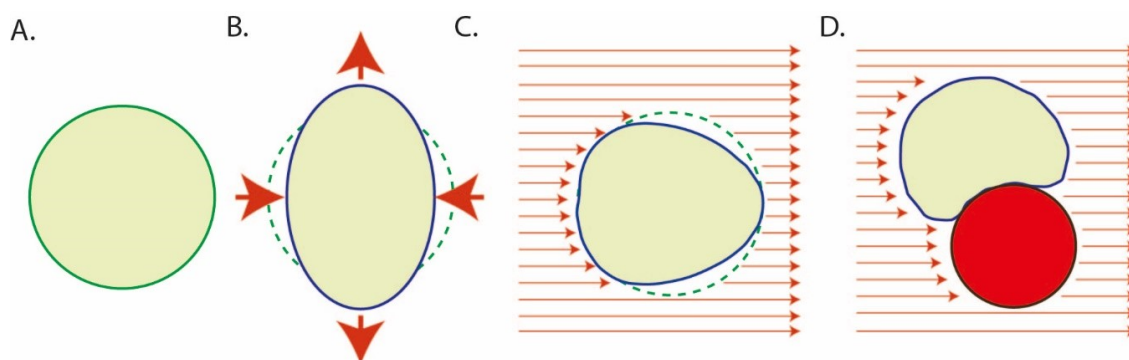


Figure 4-1 Different approaches for deforming a spherical particle

In cancer cell research, deformability has been shown to be an inherent characteristic of metastatic cells (30). Without chemical modification or molecular labeling, deformability is another label-free biomarker, which contributes as an important parameter for cell characterization and cell phenotype discrimination. All mammalian cells are deformable and have their own deformability. In a particular condition, they will be deformed in a certain shape. To measure the deformability of cells, a variety of potential techniques have been reported such as micropipette aspiration, atomic force microscopy (AFM) and optical tweezers (31), real time deformability cytometry (32). By stretching or compressing a single cell in the

optical tweezer (30) and AFM (33), a spherical cell is deformed into an elliptical shape as in Figure 4-1B. Each single cell will be independently measured and evaluated with respect to its degree of deformation. Another approach, RT-DC, was introduced in 2015 (Guck *et al.*). RT-DC has a much higher throughput (100 cells/s) (32). In a micro-channel, images of single cells were captured using a high-speed camera. Shear forces cause cells to deform into a bullet shape (Figure 4-1C). The shape of the deformed cell is used to calculate its deformability. An alternative method is a ratchet method (34), which traps cells in different levels of softness.

4.2 Deformability and Cell Sorting

An example of the similarity between cancer cells and non-cancerous cells is presented in Figure 4-2. Here, a mixture of two kinds of breast cancer cells (MCF7) and normal breast cells (MCF10A) in suspension is inspected using optical microscopy (white light and fluorescent light).

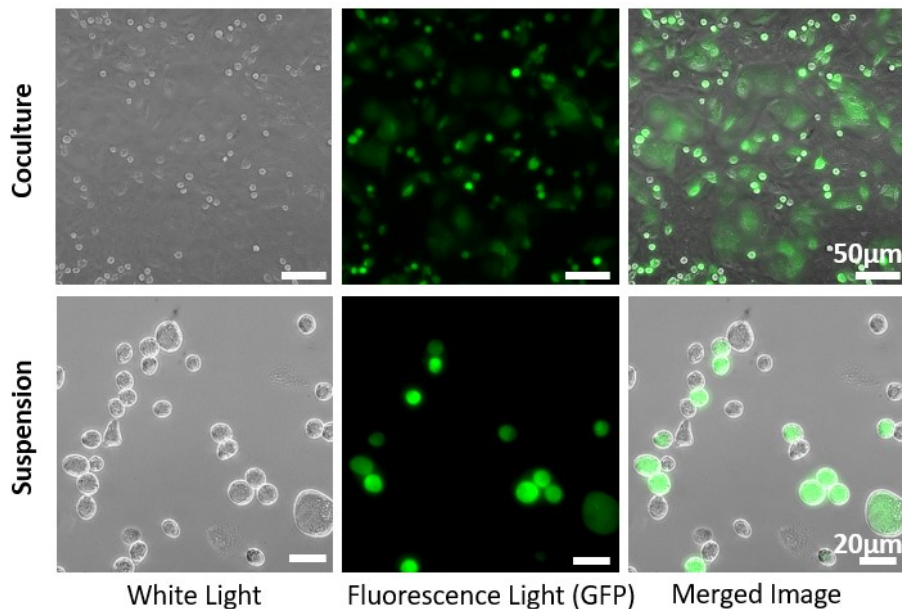


Figure 4-2 Normal and Cancer cell characteristic

Without labelling, the two cell lines are indistinguishable from one another. Size and shape measurements give a better understanding of the similarities. While the breast cancer cells have a wide distribution, which overlaps with the distribution of normal cells ($19.5 \pm 4 \mu\text{m}$ and $19.1 \pm 2 \mu\text{m}$, respectively), the circularity shows a uniform spherical shape of both cells. A significant difference between the two cell types is their propensity to form aggregates; 12 % of cells in aggregates for MCF7 and 3% for MCF10A. It is believed that cancer cell prefers to form aggregations or clusters (35).

As an introduction to the cell characteristics mentioned above, deformability is the label free marker that we aim to use for cell sorting. Especially in the DLD array where the effective sizes of particles determine their trajectories and outlet distributions. In this way, a soft particle with high deformability can change its effective size as a function of the flow rate. Figure 4-3A shows a basic idea of particle behaviors when compared to the critical size. Particle bigger than the critical size, R_c , will displace while the others follow

to the flow. In the case of soft particles, although the particle size is larger than the critical size, the effective size could be smaller (due to the deformation rate) and they behave like small particles (Figure 4-3B).

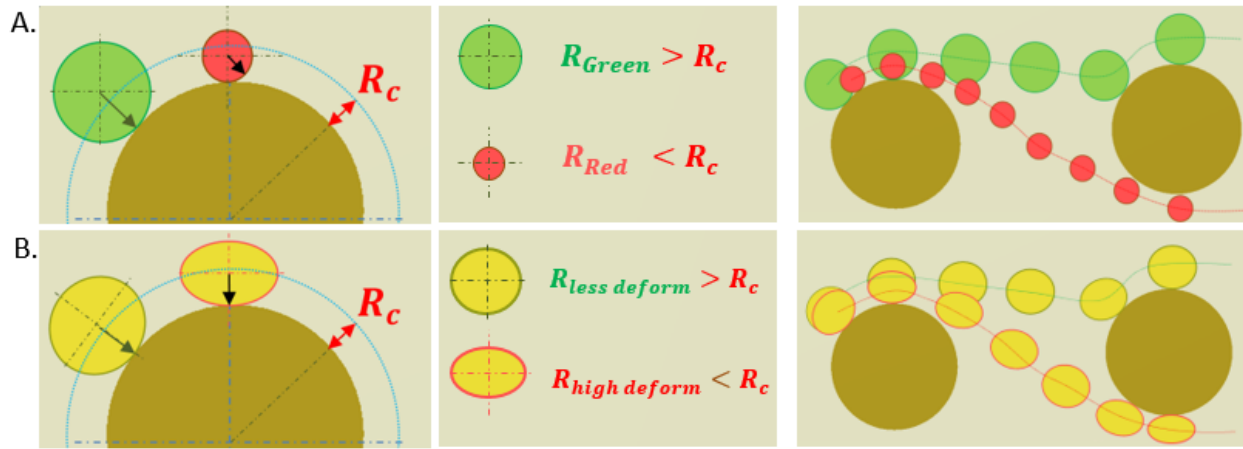


Figure 4-3 Differences of rigid and soft particles in DLD array

Biological samples are often deformable so deformability based sorting is a potential technique which can be used for the isolation or extraction of targeted cells. In this study, the main aim is to characterize and isolate the cancer cells from the normal cells based on different mechanical properties. Due to the similarities of size and shape for malignant and benign variants of many cell types, the deformability is a promising parameter for cancer-cell isolation.

Based on the measurement of MCF7 and MCF10A using the RT-DC technique, the range of deformation rate of MCF7 is observed to be wider than MCA10A. In the DLD array, the individual cells were captured and analyzed as in Figure 4-4. At low shear rates, the small particles are in zig-zag mode and the big particles are displaced following the DLD sorting mechanism. At high shear rates, the particles begin to move in the zig-zag mode, as small particles would. A typical image of an MCF7 cell when interacting with an obstacle and deforming is shown in Figure 4.4A.

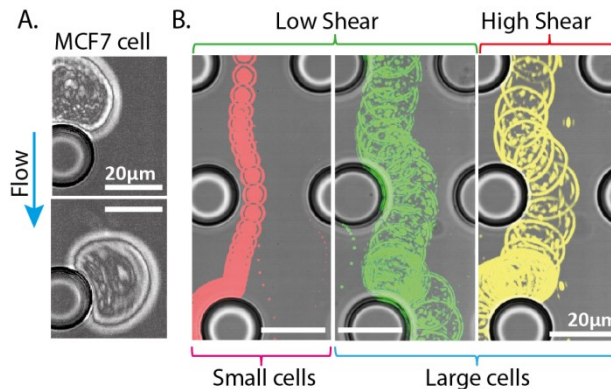


Figure 4-4 Performance of individual cells in DLD array under different shear rates

For the sorting efficiency, the outlet distribution of a population of cells is interesting to evaluate. As a function of pressure, the graph presents the distribution of each cell type and their correlation. It is

clearly observed that the distribution of cancer cells of type MCF7 is dependent on the applied pressure while the corresponding normal cells (MCF10A) are less effected. From 500mbar, the separation of cells could be obtained and give a better understanding of cell deformability.

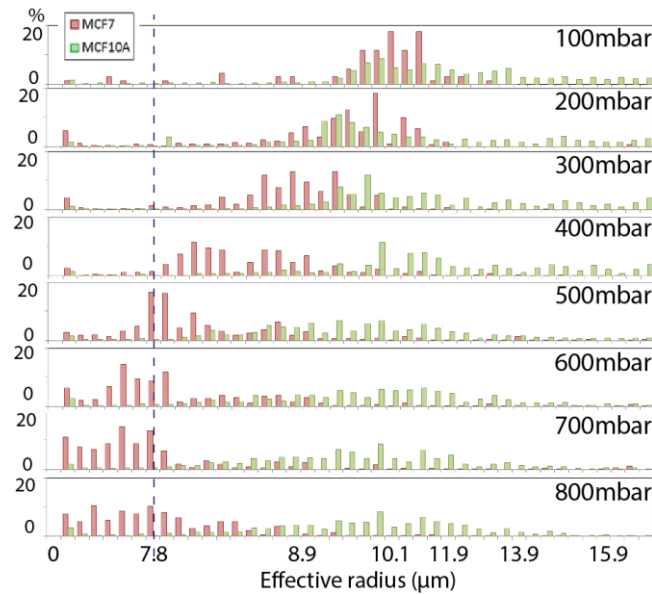


Figure 4-5 Outlet distribution of two cell types as a function of pressure

Finally, we have successfully demonstrated and measured the deformability of breast cells (MCF10A) and breast cancer cells (MCF7) using DLD devices. We find that the MCF7 cells are deformed more than 10% at the highest flow rates and that they are completely separated from the relatively much harder non-malignant cell type MCF10A.

In the next steps, the mixture of two kinds of cell will be introduced to the DLD array. As in the separated experiments, they are expected to separate at high flow rate (>100ul/min). Those cells will be collected in the resevoirs to evaluate the sorting efficiency.

Chapter 5

METHODS AND EXPERIMENTS

5.1 Device Fabrication and Sample Preparation

PDMS device fabrication

In the lithography process, a master of micro pillar array was fabricated. In a contact mask aligner (Karl Suss MJB3 and MJB4, Munich, Germany), negative photoresist SU8 (MicroChem, Newton, MA, USA) spun on a 3" silicon wafer was exposed to UV light through a chrome-mask designed in L-Edit 11.02 (Tanner Research, Monrovia, CA USA) and printed by Delta Mask (Delta Mask, Enschede, The Netherlands). Before casting of PDMS, a monolayer of 1H,1H,2H,2H-perfluorooctyl trichlorosilane (ABCR GmbH & Co. KG, Karlsruhe, Germany) was applied in the gas phase to the master as an anti-adhesion agent to facilitate demolding. A 10:1 mixture (monomer : curing agent) of PDMS (Sylgard 184, Dow Corning, Midland, MI, USA) was degassed, poured onto the master then baked for 2 hours at 80°C.

For the closed devices, PDMS stamps are punched and an oxygen plasma treatment step (Plasmatic Systems, Inc., North Brunswick, NJ, USA) is performed to enable bonding to glass slides. Silicone tubes for fluidic connections are glued to the device with silicone glue (Elastosil AO7, RTV-1 silicone rubber, Wacker Silicones, Munich, Germany). For the open device, the PDMS stamps are directly assembled with a paper pump, reservoirs (optional). A comparison of a protocol of closed DLD fabrication and optional protocol for open DLD fabrication (with and without oxygen plasma plus reservoir) is presented in Supplementary of paper 1 (Open channel DLD for particle and cell sorting).

Paper fabrication

A single and two-layer paper system were used as a capillary pump and for sample capture and collection. For liquid absorption (Herzberg flow rate 110sec/100ml), a filter paper of 0.15mm thickness, a 25-60µm pore size and 8µm particle retention (Grade 600, VWR, Sweden) was used. For sample capture, a layer of polycarbonate paper (Grade 28158, VWR, Sweden), (0.1µm pore size) was sandwiched between the separation device and the lower grade filter paper. Wax barriers were printed onto the filter paper using a wax printer (ColorQube 8570, Xerox, USA) followed by baking for 3 minutes at 100° C.

Sample preparation

Fluorescently labeled polystyrene microspheres with varying diameters (from 1 μ m to 20 μ m) (Polyscience Inc.) were suspended in milliQ water and 1% SDS and used in both closed and open DLD devices for calibration.

Soft polyacrylamide particles (diameter $15 \pm 0.84\mu$ m, Young's modulus 670 ± 280 Pa) obtained from Prof. Guck's lab (TU Dresden, Germany) were used as particle reference in softness sorting in DLD.

Small volumes of blood (10 μ l) were obtained from healthy, consenting donors via finger pricking. Blood samples were diluted 20 times in autoMACS™ running buffer (Miltenyi Biotech, Auburn, CA).

Trypanosoma cyclops parasites were thawed (after storage in 10% dimethyl sulfoxide (DMSO, Fluka, St Louis, MO: 41639) at -80°C) and cultured in Cunningham's medium 15 with 20% Fetal Calf Serum (FCS, Sigma-Aldrich) at 280C. Parasites were harvested after proliferating to cover 80% of the culture dish and spiked into blood samples.

MCF-7 (breast carcinoma cell lines obtained from the American Type Culture Collection (ATCC)) was cultured at 37°C and 5% CO₂. Cell culture medium was DMEM, 10%FBS and 1% Penicillin-Streptomycin (Sigma-Aldrich). MCF-7/GFP (breast carcinoma cell lines with Green Fluorescent Protein) (NordicBioSite) was cultured using the same protocol as the non-fluorescent MCF7.

MCF-10A (human breast cell lines obtained from the American Type Culture Collection (ATCC)) was cultured at 37°C and 5% CO₂. Cell culture medium was DMEM, 5% Horse Serum, 20ng/ml Epidermal Growth Factor (EGF), 10ug/mL Insulin, 0.5ug/mL Hydrocortisone, 100ng/mL Cholera Toxin and 1% Penicillin-Streptomycin (Sigma-Aldrich). After a one-week culture, the cells reach approximately 85-90% confluency and were considered ready for separation experiments.

5.2 Image acquisition and analysis

Particle and cell distributions were calculated from images acquired using an inverted epifluorescence microscope (Nikon Eclipse Ti, Nikon Corporation, Tokyo, Japan) and scientific CMOS camera (Flash4.0 V2, Hamamatsu, Japan).

A high-speed camera (MotionBLITZ Eosens mini, Mikrotron GmbH, Unterschleissheim, Germany), capable of capturing 10.000 frames per second, was used to obtain images of the particles and cells at high flow rates (>100ul/min).

ImageJ 1.48v software downloaded from the National Institutes of Health, and NIS-elements 4.51 were used for basic image analysis and several preparations of figures. Images of particle trajectories are generated by time-averaging and two-color images generated by adding color to separate images, taken in succession with different filter sets, and superimposing.

Matlab R2014a software was used to write image analysis code for the specific needs of cell counting and morphology detection.

All error bars of data as shown in graphs and figures were calculated by average values and standard deviation of repeated experiments.

5.3 Experiment Setup

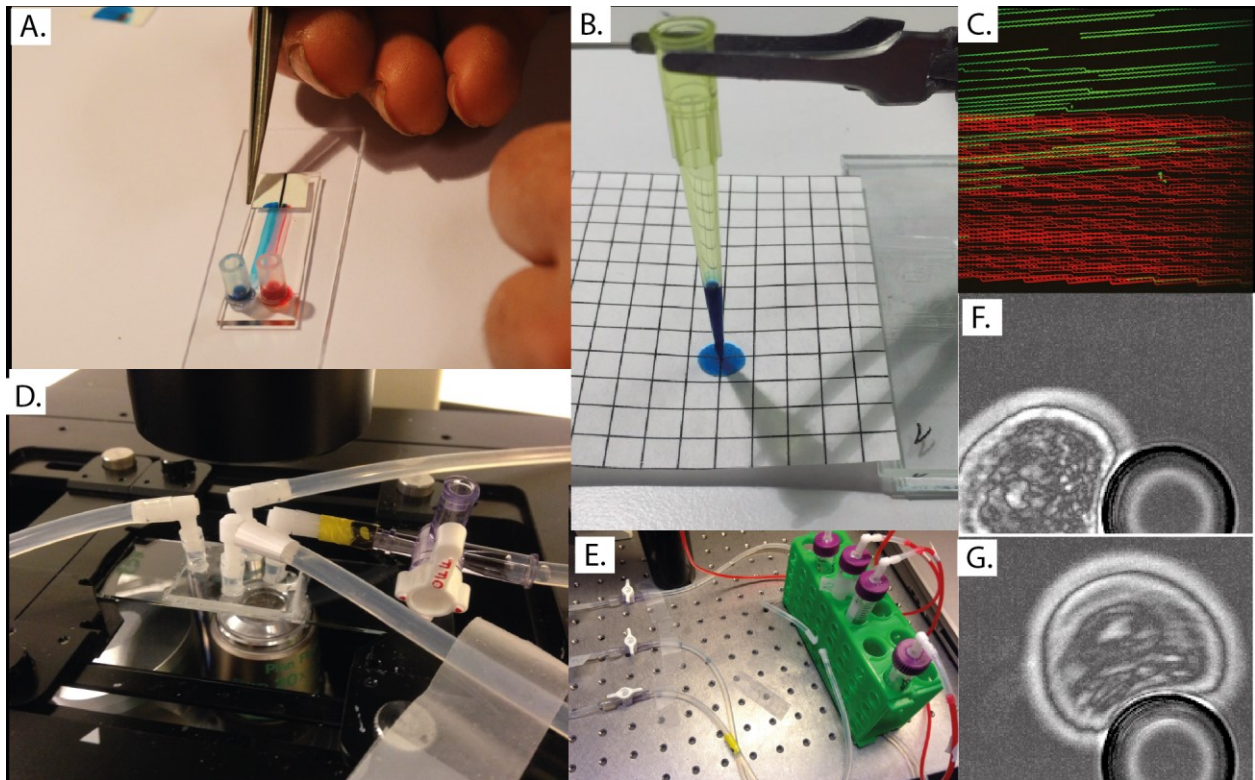


Figure 5-1 Schematic overview of all experiments in this thesis

An overview of different experimental setups is presented in Figure 5-1. From left to right, a typical experiment in open DLD system illustrates two laminar streams in the microchannel (Figure 5-1A). Secondly, a setup of a pipette tip and a filter paper presents absorption rate and expanded areas correlated to the loaded volume of food color (Figure 5-1B). A fluorescent image of particles shows a sorting ability of DLD technique (Figure 5-1C). On another hand, a complicated setup for deformability-based experiment includes tubes, connectors, valves and liquid supply system (Figure 5-1D,E). Finally, two interesting images presented cell deformation when interacting to an obstacle were captured by a high-speed camera (Figure 5-1F,G).

Chapter 6

SIGNIFICANCE STATEMENT OF MANUSCRIPTS

6.1 Open DLD Channel for Particles and Cell Sorting

We show separation of biologically relevant particles, on patterned surfaces that are reusable, based on a variety of relevant parameters such as size and shape, without the need for pumps. DLD is a proven powerful tool for bio-separations and here we show proof of principle of many of the modes of separation usually performed in single-use devices using external pumps, using easier to fabricate, reusable, simpler and therefore potentially cheaper open devices. Our approach is relevant for applications in medicine, biological research, and forensics for sample preparation and purification. The potentially low cost, ease of use and non-reliance on external equipment makes it particularly suitable for fieldwork, not least in challenging environments such as the developing world.

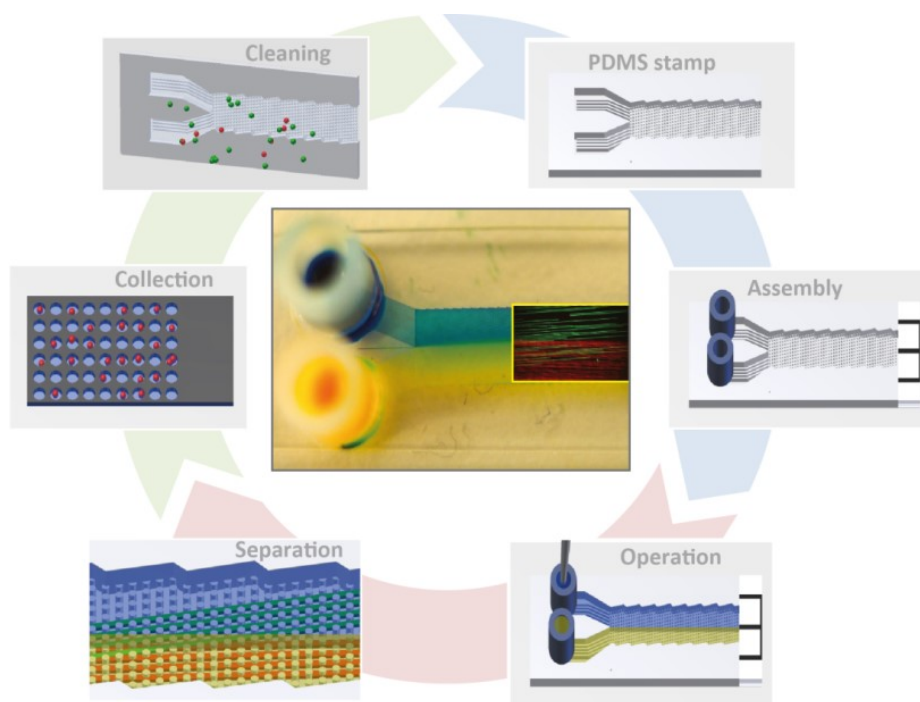


Figure 6-1 Graphical abstract for Open DLD technique

6.2 Sorting Breast Cancer Cells Based on Deformability

Due to their direct association with the physiology of the cells, the physical properties are especially attractive as markers for sorting and characterization of cancer cells. Where molecular surface markers are lacking, the physical properties can instead serve as inherent markers for separation. Specifically, this is especially interesting for cancer cells where there are indications that soft cells are more metastatic than hard cells. We have successfully demonstrated and measured the deformability of breast cells (MCF10A) and breast cancer cells (MCF7) using DLD devices. We find that the MCF7 cells are deformed more than 10% at the highest flow rates and that they are completely separated from the relatively much harder non-malignant cell type MCF10A. Proof of principle of sorting based on deformability has been shown and we will continue utilizing it for other cell types and further applications.

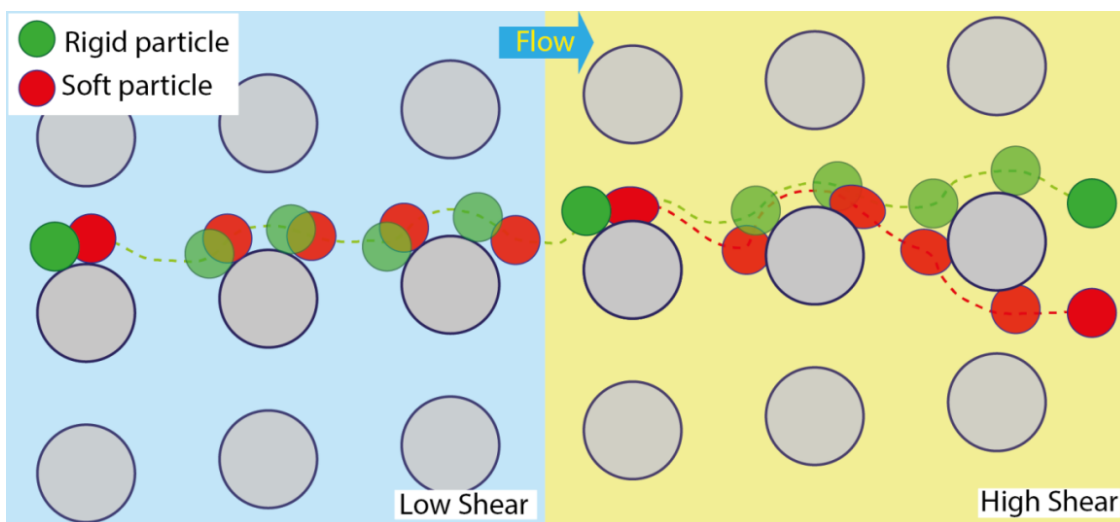


Figure 6-2 Schematic of deformability-based separation

Chapter 7

CONCLUSIONS AND OUTLOOKS

In this thesis, we successfully introduced a portable tool for particle and cell sorting by open DLD devices. With the capability to sort out various biological samples in terms of size and morphology without external equipment and specific requirements, it was proposed as a potentially useful device for conditions at resource-poor settings.

In another aspect of cell sorting, cell deformability is demonstrated as an interesting bio-marker especially when size and morphology based sorting is not sufficient to extract the specific samples of cancer cells. A proof-of-principle of cancer cell sorting using MCF7 and MCF10A cells is illustrative for deformability-based sorting using DLD.

However, the work on isolation cancer cell from the normal cells is still not yet finished. Notably, cell viability and proliferation for cells after passing through a whole DLD array need to be obtained. Furthermore, a comparison of DLD technique and FACS technique will give a better understanding of cell characteristics. Those experiments are the remaining parts of my Ph.D. projects.

In future work, more relevant cancer cells, *e.g.* clinical samples, are planned to be sorted using our techniques. To characterize the metastatic potential of the different sub-populations of the cells, transplantation of the sorted fractions in terms of size, morphology, deformability will be explored. To better understand and predict the deformability sorting, a simple theory will be developed.

The open DLD method can be further developed and put to use by integrating a reliable downstream method for identification of the sorted cells, for instance paper fluidics with specific antibodies to realize a lateral flow diagnostics devices.

Appendix

Different built-in interfaces in Matlab programming were used to analyze the above data.

- Size and shape measurement for cells (Figure 7-1)
- Cell distribution comparison of different samples (Figure 7-2)

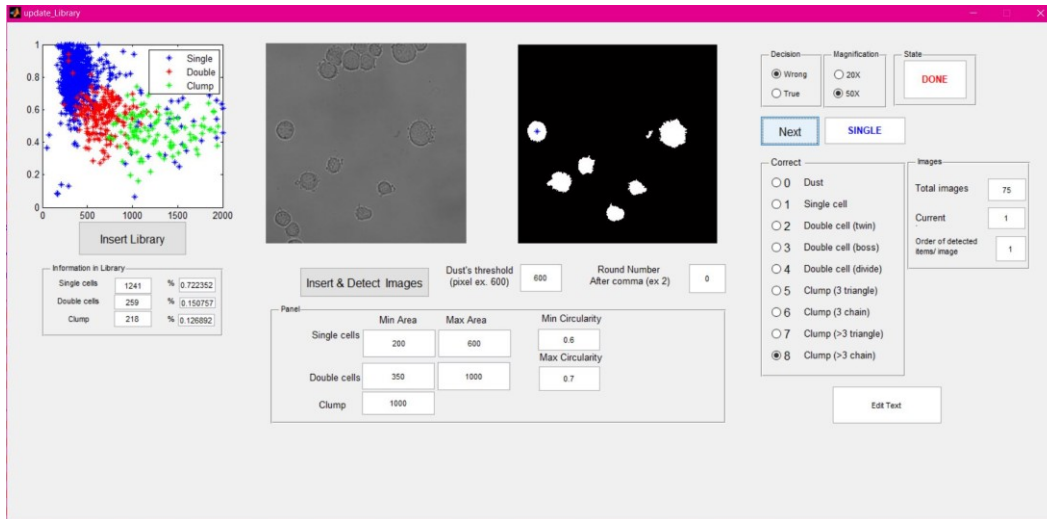


Figure 7-1 Size and shape measurement

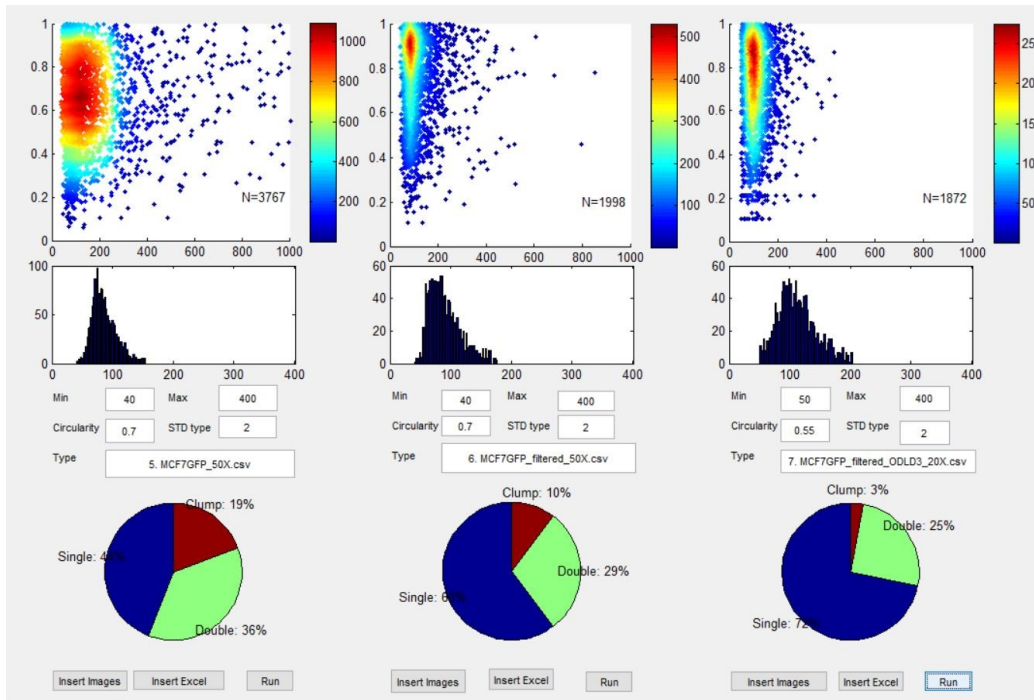


Figure 7-2 Comparison of different samples

List of the DLD devices and samples that were used in the open DLD project.

Device	Dc	Sample 1	Sample 2	Purity of Sample 1	Purity of Sample 2
DLD1	5.1 μ m	Bead 3 μ m	Bead 7 μ m	> 95%	> 95%
		RBC	Bead 3 μ m	0%	0%
		RBC	Bead 10 μ m	> 95%	> 95%
		RBC	WBC	N/A	42%
DLD2	10.7 μ m	Bead 3 μ m	Bead 16 μ m	> 95%	> 95%
		RBC	Bead 16 μ m	> 95%	> 95%
		RBC	MCF-7	> 95%	> 95%
DLD3	14.4 μ m	Bead 3 μ m	Bead 16 μ m	> 95%	> 95%
		Bead 10 μ m	Bead 15 μ m	36%	18.9%
		Bead 6 μ m	MCF-7	78.9%	92.5%
TrypDLD1	5 μ m	Trypanosome	RBC	28.4%	N/A
	9 μ m	Trypanosome	RBC	0%	0%

Bibliography

1. Craighead H (2006) Future lab-on-a-chip technologies for interrogating individual molecules. *Nature* 442(7101):387-393.
2. Shields CWt, Reyes CD, & Lopez GP (2015) Microfluidic cell sorting: a review of the advances in the separation of cells from debulking to rare cell isolation. *Lab on a chip* 15(5):1230-1249.
3. McGrath J, Jimenez M, & Bridle H (2014) Deterministic lateral displacement for particle separation: a review. *Lab on a chip* 14(21):4139-4158.
4. Terry SC, Jerman JH, & Angell JB (1979) A gas chromatographic air analyzer fabricated on a silicon wafer. *IEEE Transactions on electro devices* 26(12):1880-1886.
5. Xia Y & Whitesides GM (1998) Soft Lithography. *Angew. Chem. Int. Ed.* 37:550-575.
6. Tucker T, Marra M, & Friedman JM (2009) Massively parallel sequencing: the next big thing in genetic medicine. *American journal of human genetics* 85(2):142-154.
7. Dean SL, et al. (2013) Biorecognition by DNA oligonucleotides after exposure to photoresists and resist removers. *Langmuir : the ACS journal of surfaces and colloids* 29(36):11535-11545.
8. Cheung K, Gawad S, & Renaud P (2005) Impedance spectroscopy flow cytometry: on-chip label-free cell differentiation. *Cytometry. Part A : the journal of the International Society for Analytical Cytology* 65(2):124-132.
9. Gossett DR, et al. (2010) Label-free cell separation and sorting in microfluidic systems. *Analytical and bioanalytical chemistry* 397(8):3249-3267.
10. Huang LR, Cox EC, Austin RH, & Sturm JC (2004) Continuous particle separation through deterministic lateral displacement. *Science* 304(5673):987-990.
11. Davis JA, et al. (2006) Deterministic hydrodynamics: taking blood apart. *Proceedings of the National Academy of Sciences of the United States of America* 103(40):14779-14784.
12. Inglis DW, Lord M, & Nordon RE (2011) Scaling deterministic lateral displacement arrays for high throughput and dilution-free enrichment of leukocytes. *Journal of Micromechanics and Microengineering* 21(5):054024.
13. Civin CI, et al. (2016) Automated leukocyte processing by microfluidic deterministic lateral displacement. *Cytometry. Part A : the journal of the International Society for Analytical Cytology* 89(12):1073-1083.
14. Zeming KK, Salafi T, Chen CH, & Zhang Y (2016) Asymmetrical Deterministic Lateral Displacement Gaps for Dual Functions of Enhanced Separation and Throughput of Red Blood Cells. *Scientific reports* 6:22934.
15. Yamada M, Seko W, Yanai T, Ninomiya K, & Seki M (2017) Slanted, asymmetric microfluidic lattices as size-selective sieves for continuous particle/cell sorting. *Lab on a chip* 17(2):304-314.
16. Loutherbach K, et al. (2012) Deterministic separation of cancer cells from blood at 10 mL/min. *AIP Adv* 2(4):42107.
17. Liu Z, et al. (2013) Rapid isolation of cancer cells using microfluidic deterministic lateral displacement structure. *Biomicrofluidics* 7(1):11801.
18. Okano H, et al. (2015) Enrichment of circulating tumor cells in tumor-bearing mouse blood by a deterministic lateral displacement microfluidic device. *Biomedical microdevices* 17(3):9964.
19. Holm SH, Beech JP, Barrett MP, & Tegenfeldt JO (2011) Separation of parasites from human blood using deterministic lateral displacement. *Lab on a chip* 11(7):1326-1332.
20. Santana SM, Antonyak MA, Cerione RA, & Kirby BJ (2014) Microfluidic isolation of cancer-cell-derived microvesicles from heterogeneous extracellular shed vesicle populations. *Biomedical microdevices* 16(6):869-877.

21. Wunsch BH, *et al.* (2016) Nanoscale lateral displacement arrays for the separation of exosomes and colloids down to 20 nm. *Nature nanotechnology* 11(11):936-940.
22. Pariset E, Agache V, & Millet A (2017) Extracellular Vesicles: Isolation Methods. *Advanced Biosystems* 1(5):1700040.
23. Beech JP, Holm SH, Adolfsson K, & Tegenfeldt JO (2012) Sorting cells by size, shape and deformability. *Lab on a chip* 12(6):1048-1051.
24. Henry E, *et al.* (2016) Sorting cells by their dynamical properties. *Scientific reports* 6:34375.
25. Washburn EW (1921) The Dynamics of Capillary Flow. *Physical Review* 17(3):273-283.
26. Zimmermann M, Hunziker P, & Delamarche E (2008) Valves for autonomous capillary systems. *Microfluidics and Nanofluidics* 5(3):395-402.
27. Zimmermann M, Schmid H, Hunziker P, & Delamarche E (2007) Capillary pumps for autonomous capillary systems. *Lab on a chip* 7(1):119-125.
28. Berthier J, Brakke KA, & Berthier E (2016) *Open Microfluidics* (Wiley).
29. Beech JP & Tegenfeldt JO (2009) Capillary driven separation on patterned surfaces. *Thirteenth International Conference on Miniaturized Systems for Chemistry and Life Sciences*:785-787.
30. Guck J, *et al.* (2005) Optical deformability as an inherent cell marker for testing malignant transformation and metastatic competence. *Biophysical journal* 88(5):3689-3698.
31. Musielak M (2009) Red blood cell-deformability measurement: review of techniques. *Clin Hemorheol Microcirc* 42(1):47-64.
32. Otto O, *et al.* (2015) Real-time deformability cytometry: on-the-fly cell mechanical phenotyping. *Nature methods* 12(3):199-202, 194 p following 202.
33. Radmacher M (2007) Studying the Mechanics of Cellular Processes by Atomic Force Microscopy. 83:347-372.
34. McFaul SM, Lin BK, & Ma H (2012) Cell separation based on size and deformability using microfluidic funnel ratchets. *Lab on a chip* 12(13):2369-2376.
35. Hanahan D & Weinberg RA (2000) The Hallmarks of Cancer. *Cell* 100(1):57-70.

Paper

**Open Channel Deterministic Lateral Displacement for
Particle and Cell Sorting**



Cite this: DOI: 10.1039/c7lc00707h

Open channel deterministic lateral displacement for particle and cell sorting†

Trung S. H. Tran,  Bao D. Ho,  Jason P. Beech  and Jonas O. Tegenfeldt *

We present the use of capillary driven flow over patterned surfaces to achieve cheap and simple, but powerful separation of biologically relevant particle systems. The wide use of microfluidics is often hampered by the propensity for devices to clog due to the small channel sizes and the inability to access the interior of devices for cleaning. Often the devices can only be used for a limited duration and most frequently only once. In addition the cost and power requirements of flow control equipment limits the wider spread of the devices. We address these issues by presenting a simple particle- and cell-sorting scheme based on controlled fluid flow on a patterned surface. The open architecture makes it highly robust and easy to use. If clogging occurs it is straightforward to rinse the device and reuse it. Instead of external mechanical pumps, paper is used as a capillary pump. The different fractions are deposited in the paper and can subsequently be handled independently by simply cutting the paper for downstream processing and analyses. The sorting, based on deterministic lateral displacement, performs equivalently well in comparison with standard covered devices. We demonstrate successful separation of cancer cells and parasites from blood with good viability and with relevance for diagnostics and sample preparation. Sorting a mixture of soil and blood, we show the potential for forensic applications.

Received 6th July 2017,
Accepted 18th September 2017

DOI: 10.1039/c7lc00707h

rsc.li/loc

Introduction

Cell separation is a critical process in cell biology, disease diagnostics and prognosis. While standard techniques such as FACS and MACS are widely used, there is a need to miniaturize systems in order to minimize sample and reagent use, simplify systems for the user, and integrate components into comprehensive analysis tools. Depending on the exact applications, different types of microfluidic sorting schemes may be utilized. Inertial¹ and acoustophoretic methods² give high volumetric throughput but with a relatively low size resolution and must be operated at low particle concentrations. Deterministic lateral displacement (DLD) is a method of particle separation, based on the continuous flow of particles through an array of obstacles that exhibits exceptional resolution in size-based separations.³ DLD has been used for cell and bio-particle separations such as blood fractionation,^{4–8} trypanosome enrichment from blood,^{9,10} cancer cell isolation^{11–13} and CTC cell cluster isolation from whole blood,¹⁴ DNA and exosome separation,¹⁵ and the separation of cells based on parameters other than size, namely shape and

deformability,^{16,17} and dielectric properties.¹⁸ Early theoretical work by Inglis *et al.*¹⁹ and Davis *et al.*²⁰ describing the critical size in DLD arrays has been improved upon by studying the effects of post shape.^{21,22} Further improvements to theoretical descriptions have been made by considering other parameters such as diffusion,²³ dynamical properties,¹⁷ and alternative trajectories through DLD arrays.^{23–25} Being a passive method its basic operation does not require any application of external fields, like those used in acoustophoresis, and because it functions at high particle concentrations and low flow rates, relevant throughput can be achieved without the pressures required to generate the high particle velocities needed for inertial-effect based approaches. Even at high volume flow rates (10 mL min⁻¹) DLD has been shown to separate a variety of cells with minimal effect on viability.¹² Taken together, these qualities make DLD our method of choice for the development of a simple, cheap but effective approach to particle separation.

Here we show that by removing the lid of the DLD devices and using capillary flow we are able to perform separations, equally powerful as those in closed devices, but with many added advantages. While the benefits of open fluidics in general^{26,27} and of capillary driven DLD has been demonstrated previously,^{28,29} we here show proof of principle of their usefulness for sorting of biologically relevant particles not only based on size but also based on morphology and dielectric properties with relevance for *e.g.* medical diagnostics and

NanoLund and Division of Solid State Physics, Physics Department, Lund University, PO Box 118, 221 00, Lund, Sweden. E-mail: jonas.tegenfeldt@ftf.lth.se; Tel: +46 46 222 8063

† Electronic supplementary information (ESI) available. See DOI: 10.1039/c7lc00707h



forensics. What is more, this can be done in devices that are cheaper and easier to fabricate, since oxygen plasma and bonding is not required, and also cheaper and easier to run since pressure controllers are not required. A common limitation of standard fluidics devices, based on sealed small channels, is a propensity to clog, especially when handling complex samples. The difficulties to clean these closed devices make them unsuitable for prolonged and repeated use. We show that our open devices are easy to clean and reuse, which together with the use of the paper capillary pumps further contributes to the lowering of the costs. While standard pumps and pressure control units are ultimately more versatile, they are bulky, power consuming and expensive. We show that paper capillary pumps are compatible with open DLD devices allowing us to handle larger volumes than can fit into a device alone, and that they have the added advantage of doubling as sample collection substrates, further simplifying downstream process steps and analyses.

Results and discussion

Device fabrication and assembly

Both open and closed devices are fabricated in PDMS using replica molding on SU8 masters (see Materials and methods section). The final step in fabricating closed devices is to bond a glass slide to the PDMS cast and to then attach fluidics connectors. Open devices are much simpler in that they require neither of these two last steps. In order for the open device to function, PDMS must be rendered hydrophilic using *e.g.* oxygen plasma or, alternatively, prewetted by submersion in water. Fig. S3† in the supplementary material shows an overview of hydrophobic, hydrophilic and pre-wetted devices. Pre-wetting is much simpler to perform and negates the requirement of an oxygen plasma system, helping to keep the method cheap and simple. When a device is submerged in water the device features (channels and arrays) will fill with water after 5 minutes. When the PDMS slab is removed from submersion, water runs off of all flat areas and the only liquid remaining is that which is trapped within the patterned areas constituting the device. Sample can now be applied to the inlets and paper to the outlets and the sample will flow through the patterned areas of the device, confined to within the defined height of the features.

DLD devices in open configuration

Fig. 1A and B show a typical configuration of a closed DLD device. PDMS is bonded to glass to form closed channels and a pump or pressure control unit is used to drive flow through the device. As shown in Fig. 1C and D, our approach is to remove the glass lid and replace the pressure-driven flow with capillary flow. Provided the channels are hydrophilic, any aqueous solution placed at the inlet of the device will flow into the channels until they are filled. For our typical DLD devices (*e.g.* device 1, 20 mm length, 4 mm width and 24 μm depth, see ESI,† Fig. S1) the array volume is approximately 1.1 μL .

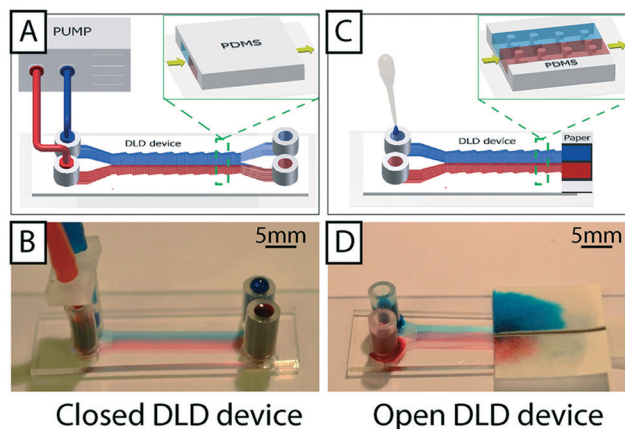


Fig. 1 Comparison of closed and open devices. (A and B) Conventional closed device where fluid is confined inside channels in a complicated setup of tubes and a pump or a pressure control unit. (C and D) Open DLD without lid. In these devices the interplay between surface tension and geometry keeps the fluid confined to the separation array and a paper reservoir at the outlet maintains flow, via capillary action, and collects the sample. We see, by observing the red and blue food coloring, that the flow is laminar in both devices.

To run the device, reservoirs are mounted at the device inlets and tested for volumes up to 60 μL using the paper capillary pump. At the beginning of the device there is a transition in liquid height from the reservoir to the bulk of the separation array. In this transition zone the sample flows across the top of the array, but the liquid height falls to that of the posts within 1–5 mm. Fig. 1D shows how we are able to maintain a stable, laminar flow (of red and blue food dye in this case) in the device using the paper capillary pump. The figure also shows how the fluids are collected in the paper. The resulting flow rates are measured to be $71 \pm 19 \text{ nL s}^{-1}$, which is comparable to what we achieve with an applied pressure of 21 mBar in a corresponding closed device. This also compares well with a closed device driven by a paper capillary pump.

The liquid in the reservoirs gives a hydrostatic pressure that is less than 1 mBar and is therefore negligible in comparison with the equivalent driving pressure in a closed device. The result is that the liquid is pulled through the device by the negative pressure imposed by the capillary pump, minimizing any liquid build-up on top of the posts.

To estimate the liquid profile along the device we resorted to three approaches. Direct imaging (Fig. 2A and B) indicates that the liquid is indeed thicker at the beginning of the device close to the reservoirs and that it levels out rather quickly away from the reservoirs. Confocal imaging supports the conclusion giving a direct view of the profile (Fig. 2C–F). Finally we studied the flow in the channels. We measure the velocities of the flow (Fig. S4B†) and combine that with the cross sectional area of the device based on the design parameters to obtain a value of the volumetric flow. The resulting flow rate is consistent with what we obtain in direct measurements of the volumetric flow rate (Fig. S5†) and measurements of the average flow by measuring the elapsed time



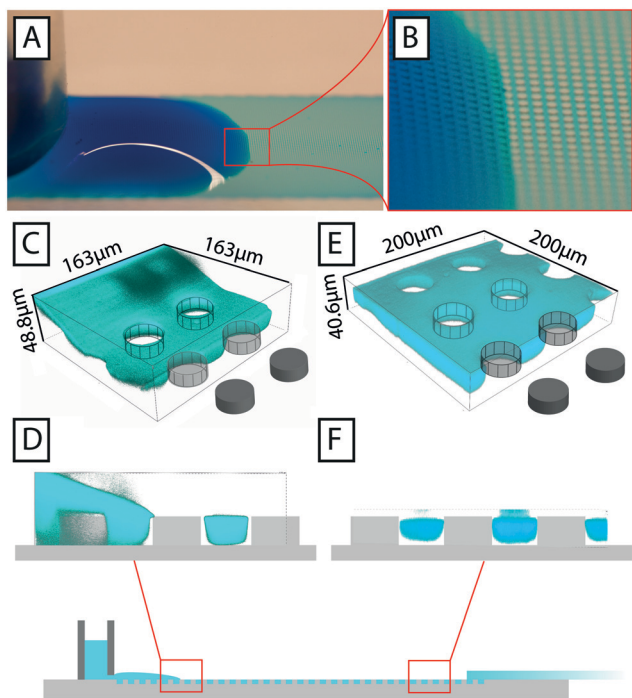


Fig. 2 Images of aqueous fluids in an open DLD device. A) Photograph of an aqueous solution of food color in an open device. B) Close-up of the transition between the area where the fluid forms a droplet and where it is confined to the post array. C) and D) 3d rendering and cross section, respectively, of confocal images of an aqueous solution of FITC in the same device, taken near to the reservoir. The drop formed by the reservoir can be seen to fall below the height of the posts. E) and F) 3d rendering and cross section, respectively, at the end of the device closest to the paper. The device is filled with liquid but no liquid can be seen above the posts.

between loading of a defined volume and the emptying of the reservoirs (Fig. S4D[†]) suggesting that the liquid is indeed filling the device to the top of the pillars. Note that there is a trend of lower flow velocities close to the reservoirs, in line with the local buildup of liquid on top of the post array that we observe by direct inspection.

The throughput of the paper capillary pump driven device is ultimately limited by the absorption rate of the paper. In a very simplified but illustrative picture the paper capillary pump can be viewed as a battery with an internal resistance and a hydromotive force in analogy to standard electrical batteries. If the external load is much less than the internal flow resistance, the flow rate is limited by the internal resistance. By measuring the flow rates in a free paper as well as a paper connected to a device (Fig. S5[†]), we could estimate the internal resistance, $16 \times 10^{12} \text{ kg s}^{-1} \text{ m}^{-4}$, which is within an order of magnitude of the resistance of our closed devices, $30 \times 10^{12} \text{ kg s}^{-1} \text{ m}^{-4}$ (from Fig. S4[†]), and open devices $23 \times 10^{12} \text{ kg s}^{-1} \text{ m}^{-4}$ (from Fig. S5[†]). From these data we could also estimate the hydromotive force to 32 mBar. Higher throughputs can now be realized by decreasing the device flow resistance through an increase in the depth of the devices or by using paper pumps with higher absorption rates. While the flow in narrow strips of paper follows the Washburn law³⁰ such that

the flow rate is inversely proportional to the square root of time, we use wider strips of paper where the liquid fans out leading to a constant flow rate as shown by Mendez *et al.*³¹ To obtain specific volumes and flow rates as a function of time, the paper capillary pumps can be programmed by selecting appropriate geometries of the paper.^{32–34} Further details on the flow generated in our open devices by the paper capillary pump can be found in the ESI.[†]

In addition to the simplifications compared to standard DLD devices we can demonstrate good separation performance. Fig. 3B shows the separation of 3 μm and 7 μm polystyrene microspheres. The sample (a mixture of the two beads) was placed in one inlet and buffer placed in the other. As the sample stream flows through the device, in parallel with the buffer stream, the mechanism of DLD causes the 7 μm particles, which are larger than the critical size, D_c , to be displaced into the buffer stream while the 3 μm particles, which are smaller than D_c remain in the sample stream. This lateral displacement is caused by steric interactions between particles and posts, which cause particles to move with a component perpendicular to the flow direction. The net result is the continuous, spatial separation of particles, Fig. 3B, in this case based on size. We also show here how the particles are collected in the paper, in regions divided by wax lines, which we will return to below. Despite the lack of a lid in our open DLD devices, flow is well defined and confined to the pillar array, and high-resolution separations can be performed fully comparable to those demonstrated for closed DLD devices. Fig. 3C shows experimental comparison of 3 devices and 10 particle sizes run in open configurations. Filled circles show particles following the flow (as expected if they are below the critical size) and open circles show those that are displaced (above the critical size). These points fall on either side of the expected critical size (indicated by red double arrows) as calculated using the empiric expressions given by Inglis *et al.*³⁵ and Davis *et al.*²⁰ for closed devices demonstrating good correspondence between particle behavior in open and closed configurations.

Application areas – proof of principle

To show the applicability of open DLD devices to relevant bio-separations, we tested separation of a range of relevant bioparticles in different modalities, as described below.

Size-based separation. Deterministic lateral displacement provides a powerful mechanism for highly precise continuous sorting based on size. In addition to the size-based separation of polystyrene beads shown above (Fig. 3) we show the separation of cells of higher biological relevance. Fig. 4A shows the size-based separation of cells from a breast cancer cell line (MCF7 cells with diameter $17.3 \pm 2.1 \mu\text{m}$) from erythrocytes (red blood cells, RBC) (diameter $7.8 \pm 0.6 \mu\text{m}$) in an open device with $D_c = 10.7 \mu\text{m}$ (device 2, see ESI,[†] Fig. S1) and Fig. 4B shows the size-based separation of white blood cells (WBC) (diameter $12.2 \pm 0.9 \mu\text{m}$) and RBCs in a device with $D_c = 5.1 \mu\text{m}$ (device 1, see ESI,[†] Fig. S1). In both cases



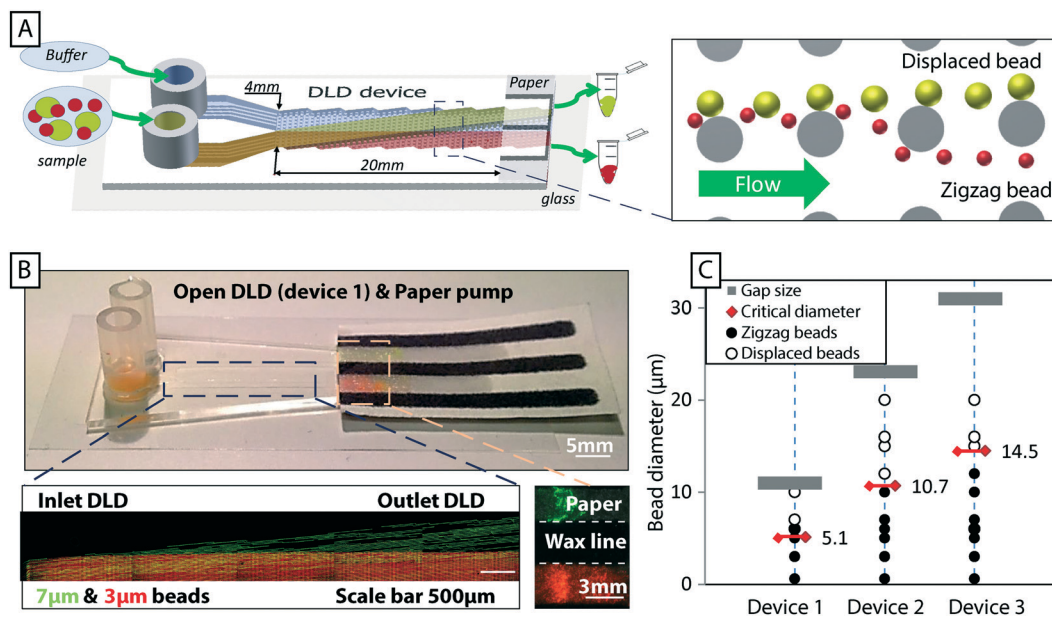


Fig. 3 An overview of open DLD, device layout and typical results. (A) Particles are introduced *via* one inlet and buffer *via* the other. The mechanism of deterministic lateral displacement pushes particles (yellow) larger than a critical size, D_c , from the sample stream to the co-flowing buffer stream as they move along the device. Smaller particles (red) remain in the sample stream. (B) Paper is used both as a capillary pump and as a method of sample collection. Here colored beads are visualized after separation and collected in zones in the paper pump defined with wax (yellow/green 7 μm and red 3 μm , black lines are wax). Time averaged images of fluorescent beads (green 7 μm and red 3 μm) in the beginning and end of the device show the trajectories of the beads in the device, which lead to separation. Note the collection of particles in separate, wax-delimited zones in the paper. (C) The behavior of open DLD devices is consistent with that of standard closed DLD devices. The red double arrows indicate theoretical critical sizes for a conventional closed device based on Davis' estimate.²⁰ The results for the open DLD are shown with filled black circles for particles in zigzag mode (following the flow), and open circles for particles in displacement mode (displaced into the buffer stream). The grey bars indicate the upper limit of the particle sizes as imposed by the gap sizes between posts.

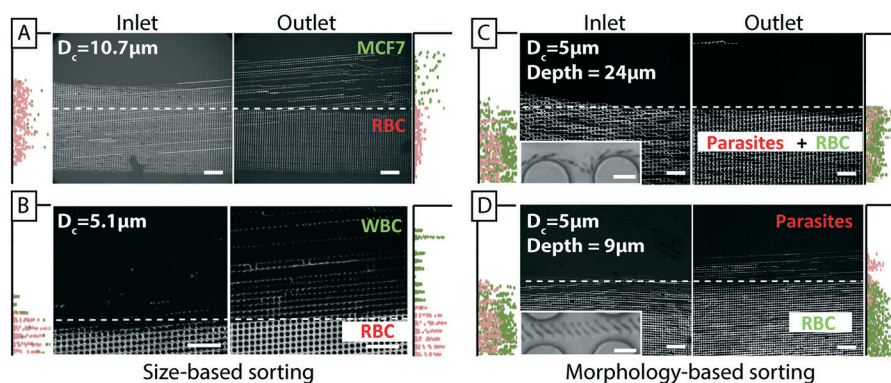


Fig. 4 Cell and parasite sorting in open DLD devices. All images show plots of inlet distributions (to the left) and outlet distributions (to the right) together with time-averaged micrographs of different cells moving through open DLD devices. The micrographs show the trajectories of the different cells in each case and the outlet distributions show the resulting separations. (A) Size-based separation of RBCs (red dots) and MCF7 cells (green dots) (B) sizebased sorting of RBCs (red dots) and WBCs (green dots) (C) in a 24 μm deep device RBCs (green dots) and parasites (*T. cyclops*) (red dots) have the same trajectories, but in a shallower device (9 μm deep) (D) they are separated. Scale bars 100 μm and 10 μm for the insets.

the performance of the devices in the simpler open configuration is equivalent to that of the same device with a lid and pressure-driven flow.

Morphology-based separation. To leverage the differences in morphology of bioparticles as a separation parameter, DLD devices can be made in which the orientation of non-spherical particles is controlled. In this way a specific aspect of the shape can be selected to influence the effective size of the particles.^{9,36} As in previous work, but now in the open de-

vice, we control the orientation of parasites to optimize their separation from erythrocytes. In a 24 μm deep device 4 (Fig. 4C), both RBCs and parasites follow the flow, whereas in a 9 μm deep device 5 (Fig. 4D) RBCs follow the flow but parasites are displaced and separation is achieved based on the same principle as was shown in ref. 9 and 36. Device parameters are shown in ESI,[†] Fig. S1.

Complex samples. We demonstrate the robustness of the open DLD by introducing a mixture of soil and blood into a



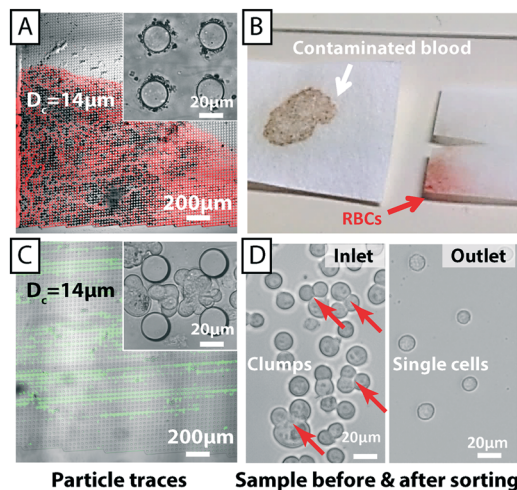


Fig. 5 Sorting of complex samples in open DLD devices. Even if large particles become trapped at the beginning of a device they do not block the flow of liquid and smaller particles as they would in a closed device. This allows extremely “dirty” samples to be analysed. A mixture of soil and RBCs is introduced into an open device. Despite the large amount of soil particles trapped at the beginning of the device (A), a clean fraction of RBCs is collected at the end of the device (B). (C) & (D) A combination of filtering and continuous separation of suspensions of cells containing large clusters that would otherwise block the inlets of a closed device.

device (Fig. 5). Soil sediments quickly and sticks in the separation array, as can be seen in Fig. 5A, but this does not cause the flow to stop. RBCs are still able to traverse the post array and a soil free fraction of RBCs is readily collected in paper at the end of the device (Fig. 5B).

A common challenge in microfluidics is the aggregation of cells that often lead to clogging even with careful surface passivation. Using the open DLD we clearly demonstrate the retention of cell aggregates of MCF7 cells while the individual cells are collected at the end of the device (Fig. 5C and D). While cell aggregates may be of interest in their own right,³⁷ in many cases, such as in cell culturing, drug screening and fluorescence activated cell sorting, it is often necessary to remove cell aggregates. Those experiments are conducted in device 3 with $D_c = 14 \mu\text{m}$ (see ESI,[†] Fig. S1).

Application of electric fields

Electrokinetic effects can be utilized in DLD devices to widen the scope and add specificities associated with the distribution of charge on the particles of interest as shown previously by Beech *et al.*¹⁸ in closed DLD devices. We added electrodes to the inlet and outlet reservoirs of a DLD device generating an electric field in the device. The electric field lines were “squeezed” between the insulating PDMS posts and field gradients were generated near the post surfaces. Polarizable particles interacted with the field gradient and the resulting dielectrophoretic (DEP) forces were used to modify the DLD-based behavior and tune size-based separations. Because there is no lid on an open device it is easy to access the fluid at any point in the device, during a separation. In the exam-

ple shown in Fig. 6 electrodes are dipped into the fluid (KCl with a conductivity of 24 mS m^{-1}) and an AC electric field is applied. In a closed device the electrodes are usually mounted in the inlet and outlet reservoirs, which are 30 mm apart in this device. Here we could easily place them 3 mm apart allowing for the generation of much higher fields at a given voltage. In Fig. 6B we see the effects of adding an electric field. In the absence of an applied voltage, $3.1 \mu\text{m}$ sulphate-terminated polystyrene and $4.8 \mu\text{m}$ carboxy-terminated polystyrene microspheres are following the flow (zigzagging), which is to be expected in a device with a critical diameter of $5.1 \mu\text{m}$ (device 1, see ESI,[†] Fig. S1), showing that the electrodes do not greatly perturb the flow. At 400 V applied AC voltage (100 Hz) the $4.8 \mu\text{m}$ microspheres are displaced and separation is achieved. At 700 V, all microspheres are displaced.

Applying electrodes in this manner, rather than in the inlets and outlets, decouples the electrode geometry from the flow geometry in a very simple way, giving us freedom to apply any number of electrodes in any pattern and at any angle to the flow direction.

Sample collection and recovery

The paper at the end of the device functions not only as a capillary pump but also as a sample recovery matrix from which fractions can be cut in a manner similar to that shown by Osborn *et al.*³⁸ Filter paper with a thickness of $150 \mu\text{m}$ and a pore size of $25\text{--}60 \mu\text{m}$ has excellent absorption. Liquid reservoirs of the required volume can be defined using a wax printer. The wax lines serve to maintain the separation of collected fractions (Fig. 1, 3 and 7). Fluorescent samples with good signal can be imaged directly in the paper with low magnification (Fig. 3 and 7). For samples with lower, or no fluorescent signal, higher magnification together with transmitted light can be used to image cells. In Fig. 7 separated MCF7 cells and RBCs are imaged inside the paper reservoirs.

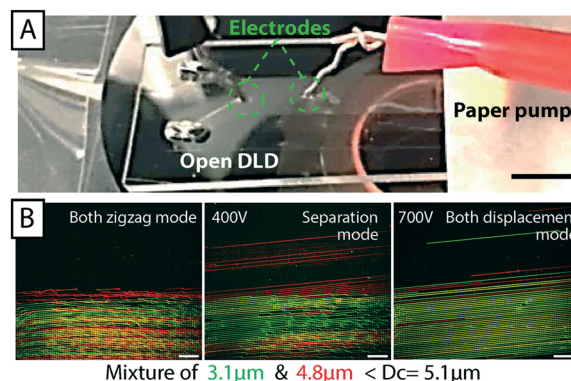


Fig. 6 Combination of electrokinetics and open DLD. (A) With direct access to the fluid it is straight-forward to position external electrodes at any point in the device. Scale bar 3 mm. An AC field at 100 Hz and various applied voltages (B) 0 V/400 V/700 V, change the trajectories of particles consistent with what was previously shown by Beech *et al.*¹⁸ in closed DLD devices. Scale bars $100 \mu\text{m}$.



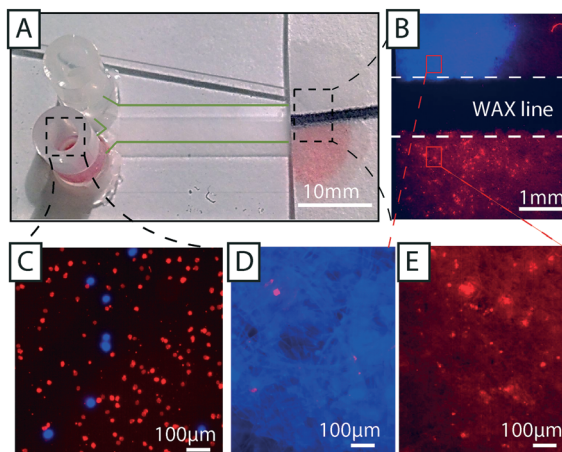


Fig. 7 Paper functions both as a capillary pump and as a collection reservoir for separated cells. (A and C) A sample containing RBCs (red fluorescence) and MCF7 cells (blue fluorescence) is introduced into an open DLD. RBCs (smaller than D_c) and MCF7 cells (larger than D_c) follow different trajectories through the device (from left to right) and can be collected to the right in two areas on the paper, separated by a printed wax line. The RBCs are more numerous than the MCF7 cells and can easily be seen in the paper through their red color (no fluorescence). Note the green dotted line that delineates the borders of the device. (B) Trapped MCF7 cells and RBCs imaged in the paper. The high concentration makes it difficult to pick out individual cells in the image, but as (D) shows, very few RBCs were observed in the top zone where the MCF7 fraction dominates. (E) No MCF7 cells are seen in the RBC fraction.

To recover cells from the paper, we have developed a simple protocol that does not negatively affect viability or proliferation (Fig. 8). The desired fractions are cut out of the paper and placed inside a liquid medium of choice

(e.g. in a 1.5 mL Eppendorf tube). Gentle vortexing releases most of the collected sample from the paper and subsequent centrifugation may then be performed to concentrate and/or collect the freed cells or particles. Fig. 8D shows a micrograph of MCF7 cells after separation in an open device, release from paper, and collection *via* centrifugation. Fig. 8E shows the recovery of 75% of cells from filter paper using this method.

While having good absorptive qualities, which is good for maintaining flow, fibrous filter paper with large pore size, is not ideal for sample collection due to trapping of particles and cells within the structure of the paper. Instead a two-layer paper system was used to increase the collection rate. By sandwiching a layer of filter membrane (1 μm pore size, polycarbonate membrane) between the filter paper and the device, the good absorptive qualities of the filter paper could be used while the polycarbonate membrane stopped the particles/cells from entering the paper and becoming trapped. Particles and cells captured on the surface of the polycarbonate membrane were easily resuspended with higher yields observed. Fig. 8E shows how 95% of cells could be recovered using the extra membrane layer.

To measure the effect of sorting in both open and closed devices on the health of cells, we performed viability and proliferation assays of MCF7 cells. Cell counting using viability dyes (trypan blue) was conducted to measure the percentage of viable cells and the rate of proliferation. Fig. 8F demonstrates viabilities of >90% for sorted cells. A small difference in the viability of cells (control, open, and closed devices) could be seen in our measurements but the difference has no practical significance and shows nothing more than the

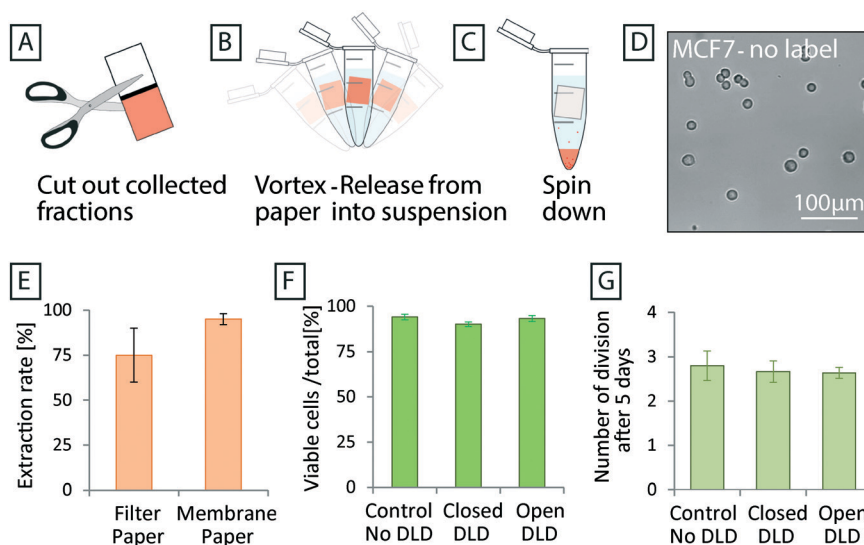


Fig. 8 Post-separation sample recovery. (A) Separated fractions are accumulated in the paper and kept separated by hydrophobic wax lines. The desired fractions are collected separately by dividing the paper along the wax line. (B) To re-suspend the collected fractions vortexing is used, followed by (C) centrifugation. (D) MCF7 cells after separation and collected using the process described in (A)–(C). (E) Recovery statistics for the filter paper and the two-layer system. Error bars show max/min values from 5 experiments. (F) Cell viability and (G) proliferation assay for MCF7 after separation in closed and open DLD. Error bars show the standard deviation in (F) and (G). No significant difference could be seen in the proliferation rates of sorted and non-sorted cells.



common variation between cultures using these cells. Furthermore, Fig. 8G shows that after 5 days of culturing, no difference in the proliferation rates of cells, (~ 2.5 divisions in 5 days), can be seen as a consequence of sorting.

The performance of the devices is qualitatively comparable to the conventional closed devices with clear separation of the different fractions. Purity and capture rate are performance parameters that do not depend on the DLD as much as on the overall design and will have to be optimized carefully for each specific application. For example the paper capillary pump in Fig. 3B can be extended to three lanes instead of two. In that way the purity of the sample collected in the two extreme lanes can be enhanced by discarding the central lane. The data in Fig. 4 shows clearly that by appropriate choice of cut-offs we would be able to achieve close to 100% purity of the separated fractions. With longer devices, this is expected to be done with minimum loss of capture efficiency.

Cleaning and reusing devices

The fouling of devices with particles and cells is the most common reason for device failure and limits device lifetime. Fouling can be due to several mechanisms. Particles can adhere to surfaces and they can become trapped because they are too large to move through constrictions. These mechanisms are also linked. For example, particles can stick to one another, forming agglomerations that are much more likely to get stuck. Fig. 9A shows an image of 4.5 and 10 μm particles that have become stuck in a closed device with a $D_c = 5.1 \mu\text{m}$ and gap size of 11 μm after operating for 30 min (device 1, see ESI,† Fig. S1). At this point the device has ceased to

work and particles are no longer able to enter the array. This kind of clogging is detrimental for all kinds of microfluidics devices, in particular for DLD devices since a well-defined flow direction is crucial for the successful operation. Even a small deviation of flow direction may change the critical size significantly.

Closed devices are most often irreversibly sealed (to avoid leaking) and are difficult to clean and reuse. Fig. 9B shows the same device after sonication, reversal of the flow direction and an increase in pressure in an effort to remove clogging. Despite these efforts many particles remain stuck in the device and the device is unusable. Open devices are considerably easier to clean and can be cleaned to a much higher degree. Fig. 9C shows the same kind of device as above after first being run in an open configuration and then cleaned by sonication and rinsing. This device is free of particles after rinsing and can be reused.

Conclusion

We have shown that by combining patterned surfaces in PDMS with paper based capillary pumps we can fabricate potentially cheap, simple to use, and reusable continuous flow separation devices. We have demonstrated proof-of-principle separations of samples based on size and morphology and what is more, in samples containing very large contaminant particles. Being open, access to flowing fluid is possible in these devices allowing for easy electric contact through electrodes. Flow rates can be held constant by choice of size and properties of the paper used in the capillary pump. Paper is not only useful as a pump but also as a matrix for the collection of separated fractions. The separational functionality of DLD is retained in open devices paving the way for simple, robust and clogging insensitive sorting using pillar arrays with potential applications in medicine and forensic science. Our device opens up for sample preparation applications in paper fluidics based diagnostics.^{39,40}

The limitations and challenges introduced by working with open devices on the other hand include the risk for evaporation, contamination and biohazard.⁴¹ These issues can be mitigated through a cover that is positioned in close proximity, yet not in contact with the actual device.

Materials and methods

PDMS device fabrication

In a contact mask aligner (Karl Suss MJB3 and MJB4, Munich, Germany), negative photoresist SU8 (MicroChem, Newton, MA, USA) spun on a 3" silicon wafer was exposed with UV light through a chrome-mask designed in L-Edit 11.02 (Tanner Research, Monrovia, CA USA) and printed by Delta Mask (Delta Mask, Enschede, The Netherlands). Before casting of PDMS, a monolayer of 1H,1H,2H,2H-perfluorooctyltrichlorosilane (ABCR GmbH & Co. KG, Karlsruhe, Germany) was applied in the gas phase to the master

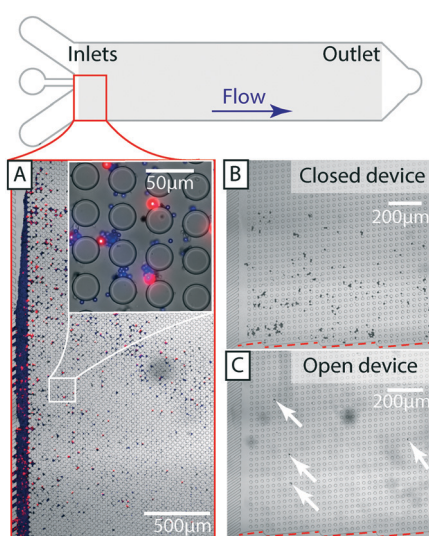


Fig. 9 Cleaning and reusing open DLD devices. (A) Depending on the array parameters, particle sizes and surface chemistries, devices eventually clog. (B) A closed device after attempted cleaning using sonication, high pressures and reversing the flow direction. (C) An open device after sonication and rinsing is almost completely free of particles (30 times fewer). Those remaining are highlighted with arrows. Channel walls are shown in red dashed lines.



as an anti-adhesion agent to facilitate demoulding. A 10:1 mixture (monomer:curing agent) of PDMS (Sylgard 184, Dow Corning, Midland, MI, USA) was degassed, poured onto the master then baked for 2 hours at 80 °C. For the closed devices vias are punched and an oxygen plasma treatment step (Plasma Preen II-862, Plasmatic Systems, Inc., North Brunswick, NJ, USA) is performed to enable bonding to glass slides and the attaching of silicone tubes for fluidic connections, none of which are necessary for the open devices. In Fig. S2† (supplementary of device fabrication), a comparison among a protocol of closed DLD fabrication and optional protocol for open DLD fabrication (with and without oxygen plasma plus reservoir) is presented.

Paper capillary pump

A two-layer paper system was used as a capillary pump and for sample capture and collection for the experiments described in Fig. 8. For liquid absorption (Herzberg flow rate⁴² 110 s/100 mL), filter paper of 0.15 mm thickness, a 25–60 µm pore size and 8 µm particle retention (Grade 600, VWR, Sweden) was used. For sample capture a layer of polycarbonate paper (Grade 28158, VWR, Sweden), (1 µm pore size) was sandwiched between the separation device and the lower grade filter paper. For the other experiments only the filter paper was used. Wax barriers were printed onto the filter paper using a wax printer (ColorQube 8570, Xerox, USA) followed by baking for 3 minutes at 100 °C.

For the experiments characterizing the evaporation, a grid was printed onto the paper to facilitate measurement of the wetted area. The grid was printed using a standard laser writer (Canon iR-ADV C5250i).

Sample preparation (beads, RBCs, WBCs and MCF7 cells)

Fluorescently labeled polystyrene microspheres with varying diameters (from 1 µm to 20 µm) (Polyscience Inc., Warrington, PA, USA) were suspended in MilliQ water and 1% SDS and used in both closed and open DLD devices for calibration.

Small volumes of blood (10 µL) were obtained from healthy, consenting donors *via* finger pricking. Blood samples were diluted 20 times in autoMACS™ running buffer (Miltenyi Biotec, Auburn, CA, USA).

Trypanosoma cyclops parasites were thawed (after storage in 10% dimethyl sulfoxide (DMSO, Fluka, St. Louis, MO, USA: 41639) at –80 °C) and cultured in Cunningham's medium with 20% fetal calf serum (FCS, Sigma-Aldrich) at 28 °C. Parasites were harvested after proliferating to cover 80% of the culture dish and spiked into blood samples.

MCF-7 (breast carcinoma cell lines obtained from the American Type Culture Collection (ATCC)) was cultured at 37 °C and 5% CO₂. Cell culture medium was Dulbecco's modified Eagle's medium (DMEM), 10% FBS and 1% penicillin streptomycin (Sigma-Aldrich). After one week of subculture,

the cells proliferated to fill more than 80% of the culture flasks and were considered ready for separation experiments.

Image acquisition and analysis

Particle and cell distributions were calculated from images acquired using an inverted epifluorescence microscope (Nikon Eclipse Ti, Nikon Corporation, Tokyo, Japan) and scientific CMOS camera (Flash4.0 V2, Hamamatsu, Japan). ImageJ 1.48v software downloaded from the National Institutes of Health, and NIS-elements 4.51 were used for image analysis and the preparation of figures. Images of particle trajectories are generated by time-averaging. Two color-images generated by adding color to separate images, taken in succession with different filter sets, and superimposing.

Conflicts of interest

There are no conflicts to declare.

Acknowledgements

We thank Stefan Holm and Bo Baldetorp for their kind donation of trypanosomes and MCF-7 cells respectively. This work was carried out within NanoLund at Lund University with funding from the Child Cancer Foundation (MT2013-0031), LAPASO (EU FP7 project 607350) and the Swedish Research Council (VR) grant no. 2015-05426. All device processing was conducted within Lund Nano Lab. We thank Christelle Prinz for valuable comments after carefully reading the manuscript.

References

- 1 D. Di Carlo, D. Irimia, R. G. Tompkins and M. Toner, *Proc. Natl. Acad. Sci. U. S. A.*, 2007, **104**, 18892–18897.
- 2 T. Laurell, F. Petersson and A. Nilsson, *Chem. Soc. Rev.*, 2007, **36**, 492–506.
- 3 L. R. Huang, E. C. Cox, R. H. Austin and J. C. Sturm, *Science*, 2004, **304**, 987–990.
- 4 J. A. Davis, D. W. Inglis, K. J. Morton, D. A. Lawrence, L. R. Huang, S. Y. Chou, J. C. Sturm and R. H. Austin, *Proc. Natl. Acad. Sci. U. S. A.*, 2006, **103**, 14779–14784.
- 5 D. W. Inglis, M. Lord and R. E. Nordon, *J. Micromech. Microeng.*, 2011, **21**, 054024.
- 6 C. I. Civin, T. Ward, A. M. Skelley, K. Gandhi, Z. P. Lee, C. R. Dosier, J. L. D'Silva, Y. Chen, M. Kim, J. Moynihan, X. C. Chen, L. Aurich, S. Gulnik, G. C. Brittain, D. J. Recktenwald, R. H. Austin and J. C. Sturm, *Cytometry, Part A*, 2016, **89A**, 1073–1083.
- 7 K. K. Zeming, T. Salafi, C. H. Chen and Y. Zhang, *Sci. Rep.*, 2016, **6**, 22934.
- 8 M. Yamada, W. Seko, T. Yanai, K. Ninomiya and M. Seki, *Lab Chip*, 2017, **17**, 304–314.
- 9 S. H. Holm, J. P. Beech, M. P. Barrett and J. O. Tegenfeldt, *Lab Chip*, 2011, **11**, 1326–1332.
- 10 S. H. Holm, J. P. Beech, M. P. Barrett and J. O. Tegenfeldt, *Anal. Methods*, 2016, **8**, 3291–3300.



- 11 Z. B. Liu, F. Huang, J. H. Du, W. L. Shu, H. T. Feng, X. P. Xu and Y. Chen, *Biomicrofluidics*, 2013, 7, 011801.
- 12 K. Loutharback, J. D'Silva, L. Y. Liu, A. Wu, R. H. Austin and J. C. Sturm, *AIP Adv.*, 2012, 2, 042107.
- 13 H. Okano, T. Konishi, T. Suzuki, T. Suzuki, S. Ariyasu, S. Aoki, R. Abe and M. Hayase, *Biomed. Microdevices*, 2015, 17, 59.
- 14 S. H. Au, J. Edd, A. E. Stoddard, K. H. K. Wong, F. Fachin, S. Maheswaran, D. A. Haber, S. L. Stott, R. Kapur and M. Toner, *Sci. Rep.*, 2017, 7, 2433.
- 15 B. H. Wunsch, J. T. Smith, S. M. Gifford, C. Wang, M. Brink, R. L. Bruce, R. H. Austin, G. Stolovitzky and Y. Astier, *Nat. Nanotechnol.*, 2016, 11, 936–940.
- 16 J. P. Beech, S. H. Holm, K. Adolfsson and J. O. Tegenfeldt, *Lab Chip*, 2012, 12, 1048–1051.
- 17 E. Henry, S. H. Holm, Z. M. Zhang, J. P. Beech, J. O. Tegenfeldt, D. A. Fedosov and G. Gompper, *Sci. Rep.*, 2016, 6, 34375.
- 18 J. P. Beech, P. Jonsson and J. O. Tegenfeldt, *Lab Chip*, 2009, 9, 2698–2706.
- 19 D. W. Inglis, J. A. Davis, R. H. Austin and J. C. Sturm, *Lab Chip*, 2006, 6, 655–658.
- 20 J. A. Davis, *Doctoral thesis*, Princeton, 2008.
- 21 Z. Zhang, E. Henry, G. Gompper and D. A. Fedosov, *J. Chem. Phys.*, 2015, 143, 243145.
- 22 K. Loutharback, K. S. Chou, J. Newman, J. Puchalla, R. H. Austin and J. C. Sturm, *Microfluid. Nanofluid.*, 2010, 9, 1143–1149.
- 23 B. R. Long, M. Heller, J. P. Beech, H. Linke, H. Bruus and J. O. Tegenfeldt, *Phys. Rev. E*, 2008, 78, 046304.
- 24 J. Frechette and G. Drazer, *J. Fluid Mech.*, 2009, 627, 379–401.
- 25 S. C. Kim, B. H. Wunsch, H. Hu, J. T. Smith, R. H. Austin and G. Stolovitzky, *Proc. Natl. Acad. Sci. U. S. A.*, 2017, 114, E5034–E5041.
- 26 J. Melin, W. van der Wijngaart and G. Stemme, *Lab Chip*, 2005, 5, 682–686.
- 27 B. P. Casavant, E. Berthier, A. B. Theberge, J. Berthier, S. I. Montanez-Sauri, L. L. Bischel, K. Brakke, C. J. Hedman, W. Bushman, N. P. Keller and D. J. Beebe, *Proc. Natl. Acad. Sci. U. S. A.*, 2013, 110, 10111–10116.
- 28 J. P. Beech and J. O. Tegenfeldt, Capillary driven separation on patterned surfaces, *microTAS 2009, The 13th International Conference on Miniaturized Systems for Chemistry and Life Sciences*, Jeju, Korea, November 1–5, 2009, pp. 785–787.
- 29 K. Morton, O. K. C. Tsui, C. K. Tung, J. C. Sturm, S. Y. Chou and R. Austin, *New J. Phys.*, 2010, 12, 085008.
- 30 E. W. Washburn, *Phys. Rev.*, 1921, 17, 273–283.
- 31 S. Mendez, E. M. Fenton, G. R. Gallegos, D. N. Petsev, S. S. Sibbett, H. A. Stone, Y. Zhang and G. P. Lopez, *Langmuir*, 2010, 26, 1380–1385.
- 32 E. Elizalde, R. Urteaga and C. L. Berli, *Lab Chip*, 2015, 15, 2173–2180.
- 33 P. Yager, T. Edwards, E. Fu, K. Helton, K. Nelson, M. R. Tam and B. H. Weigl, *Nature*, 2006, 442, 412–418.
- 34 B. M. Cummins, R. Chinthapatla, B. Lenin, F. S. Ligler and G. M. Walker, *Technology*, 2017, 5, 21–30.
- 35 D. W. Inglis, J. A. Davis, R. H. Austin and J. C. Sturm, *Lab Chip*, 2006, 6, 655–658.
- 36 S. H. Holm, J. P. Beech, M. P. Barrett and J. O. Tegenfeldt, *Anal. Methods*, 2016, 8, 5726–5726.
- 37 A. F. Sarioglu, N. Aceto, N. Kojic, M. C. Donaldson, M. Zeinali, B. Hamza, A. Engstrom, H. Zhu, T. K. Sundaresan, D. T. Miyamoto, X. Luo, A. Bardia, B. S. Wittner, S. Ramaswamy, T. Shioda, D. T. Ting, S. L. Stott, R. Kapur, S. Maheswaran, D. A. Haber and M. Toner, *Nat. Methods*, 2015, 12, 685–691.
- 38 J. L. Osborn, B. Lutz, E. Fu, P. Kauffman, D. Y. Stevens and P. Yager, *Lab Chip*, 2010, 10, 2659–2665.
- 39 Y. Yang, E. Noviana, M. P. Nguyen, B. J. Geiss, D. S. Dandy and C. S. Henry, *Anal. Chem.*, 2017, 89, 71–91.
- 40 K. Yamada, H. Shibata, K. Suzuki and D. Citterio, *Lab Chip*, 2017, 17, 1206–1249.
- 41 Y. Temiz, R. D. Lovchik, G. V. Kaigala and E. Delamarque, *Microelectron. Eng.*, 2015, 132, 156–175.
- 42 W. Herzberg, *Papierprüfung*, Springer, Berlin, Heidelberg, 1921, p. 109, DOI: 10.1007/978-3-662-25211-6_18.



Open Channel Deterministic Lateral Displacement for Particle and Cell Sorting

Trung S.H. Tran, Bao D. Ho, Jason P. Beech and Jonas O. Tegenfeldt

Electronic Supporting Information

Design and fabrication

The basic operational principle of DLD along with relevant parameters and critical separation diameters for our DLD devices are shown in Figure S1.

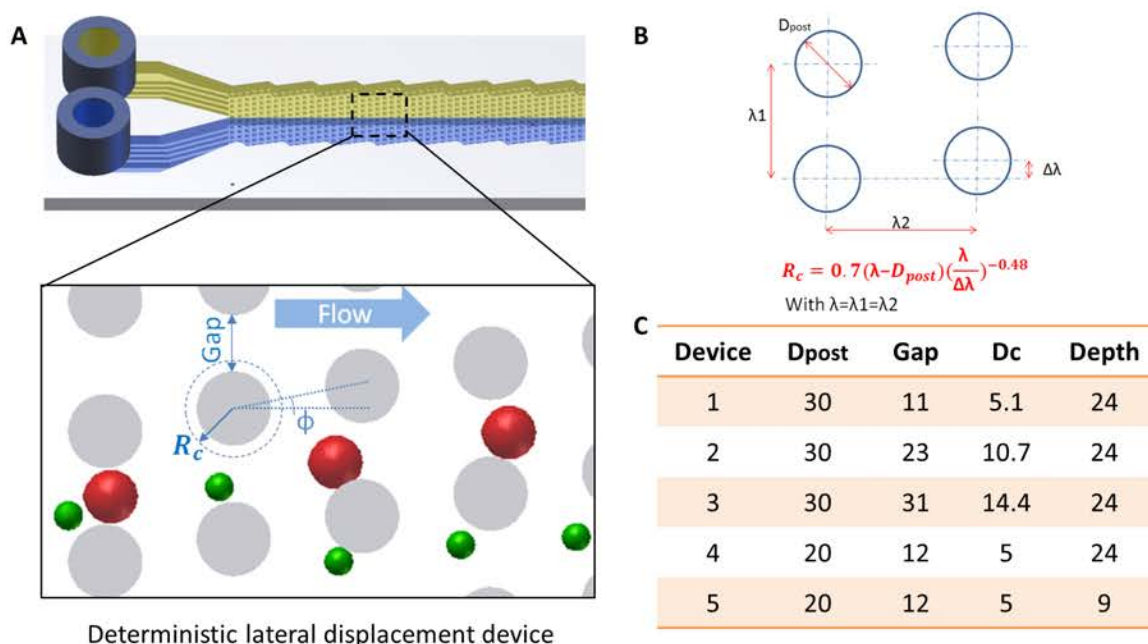


Figure S1. (A) Schematic of a typical DLD device with particle trajectories, (B) Key parameters determining the critical diameter (D_c) of a DLD array, (C) List of DLD devices used in this report (length units are μm). Length of the devices is 20 mm and width is 4 mm.

Several fabrication and surface treatment schemes were tested for our devices (Figure S2). Figure S2A shows the conventional method of fabricating closed PDMS/glass devices with a plasma-bonding step (that also renders the PDMS hydrophilic) and the attachment of reservoirs/pressure control connections.

Preparation of devices

For the open devices, if a drop of aqueous solution is applied at the end of an untreated (hydrophobic) DLD array, the droplet will stay on the surface and will not wet the channels or array area of the device. This can be overcome in two ways. Figure S2B shows an open device in which the channels are selectively rendered hydrophilic by use of a mask during oxygen plasma treatment. The untreated, hydrophobic PDMS surrounding the active area of the device serves to confine the sample, which would otherwise spread outside the features of the device. Another approach, that is simpler because oxygen plasma is not needed, is

shown in Figures S2C and D. By submerging the device in an aqueous solution (1% SDS for polystyrene bead sorting, AutoMacs™ for RBC, and complete Dulbecco’s Modified Eagle’s Medium (DMEM) for cancer cell experiments) at room temperature for 5 minutes, the entire surface of the device can be forced to wet. When the device is removed from the solution the flat PDMS surface is sufficiently hydrophobic to repel the aqueous solution, but the water inside the structures of the device remains. After the positioning of the paper capillary pump at the outlet and the addition of more sample at the inlet, flow is maintained and separation can be performed. The reservoir, shown in Figure S2D, is not essential but allows for greater control of the sample and the handling of larger sample volumes.

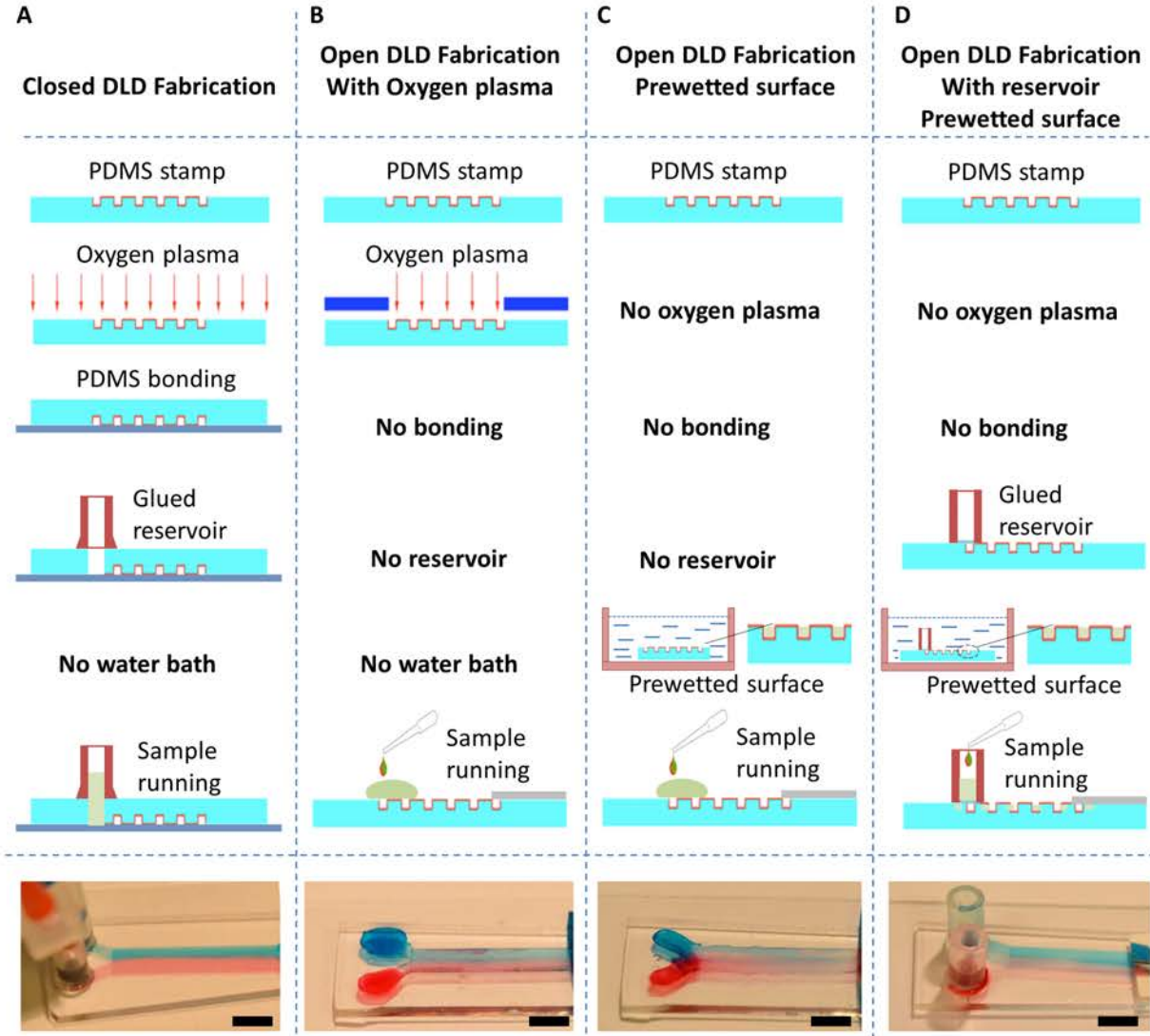


Figure S2. Comparison of different fabrication methods for closed and open DLD devices. (A) Conventional closed device fabrication. (B) Open device where the sorting structures are selectively treated with oxygen plasma to make them hydrophilic. (C) Rendering the PDMS hydrophilic by immersion (prewetting) in a water bath (plain water at room temperature in 5 minutes) instead of in an oxygen plasma. (D) Addition of a reservoir gives better control of the sample and allows for larger volumes. Scale bars 5 mm.

The wetting of the devices using the different surface treatment strategies was characterized in more detail as presented in Figure S3. Selective oxygen plasma treatment gives a strongly hydrophilic surface with contact angle $\sim 0^\circ$. Immersing the device in aqueous buffer gives a less hydrophilic surface (contact angle $\sim 60^\circ$ outside the device and an effective contact angle $\sim 0^\circ$ in the DLD array). The latter approach is fully adequate for the operation of the device and much simpler as it does not require any oxygen plasma equipment.

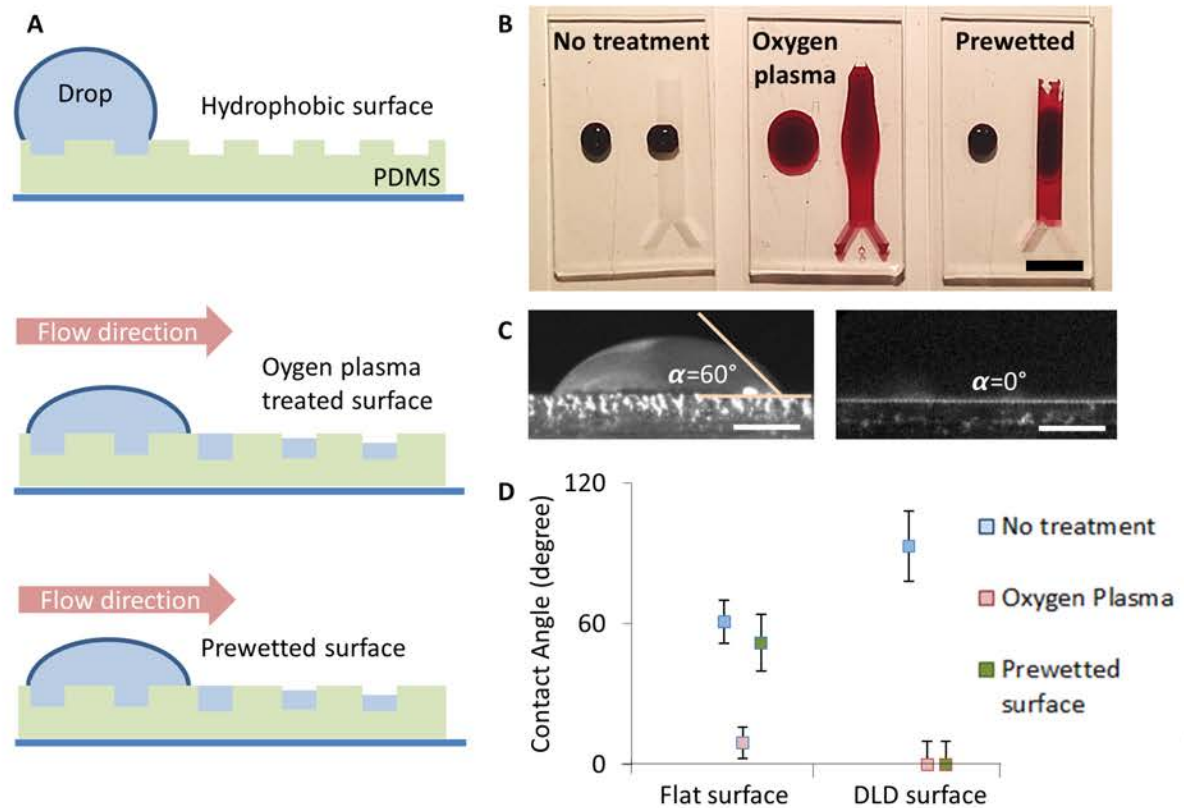


Figure S3. Hydrophobic and hydrophilic devices. (A) Schematic of a water droplet on an untreated (hydrophobic) surface and the two treated hydrophilic surfaces (B) Visualization of the wetting behavior of the three kinds of surface treatments on flat and patterned PDMS using an aqueous solution of red food coloring. (C) Cross-sectional view of water drop outside and on the DLD array for a prewetted surface. (D) Comparison of wetting angles on flat and patterned surfaces after no treatment, oxygen plasma and prewetting. The error bars represent the standard deviation of the measurement.

Volume of a filled device

The volume of the liquid in a filled device is calculated based on the table in figure S1C. The ratio of the area of the fluid and the total area of the unit cell is 0.58, which is multiplied with the overall dimensions of the device (length 20 mm, width 4 mm and depth 24 μm), giving us the total volume of device 1 of 1.1 μL .

Uniformity of wetting

The characteristics and uniformity of the wetted array are characterized by confocal microscopy and direct imaging with a macro objective. In both cases device 3 was used with added reservoirs. For the confocal images fluorescein isothiocyanate (FITC) was first dissolved in methanol to 10% that was in turn diluted in water 100 times and the methanol

allowed to evaporate. The confocal microscope is based on a Yokogawa CSU22 spinning disc, Andor laser combiner and Andor iXon DU-897 CCD camera on an inverted Nikon Ti microscope. A Plan 50x ELWD Dry and a Plan Fluor ELWD 40x Ph2 ADL objective with NA 0.32 and 0.4 respectively were used for figures 2C-F. Since the microscope is inverted, the device was turned upside-down for imaging (surface tension dominates and so this has little to no effect on the shape of the liquid surface). The image contrast was adjusted such that scattered light was rejected from the image.

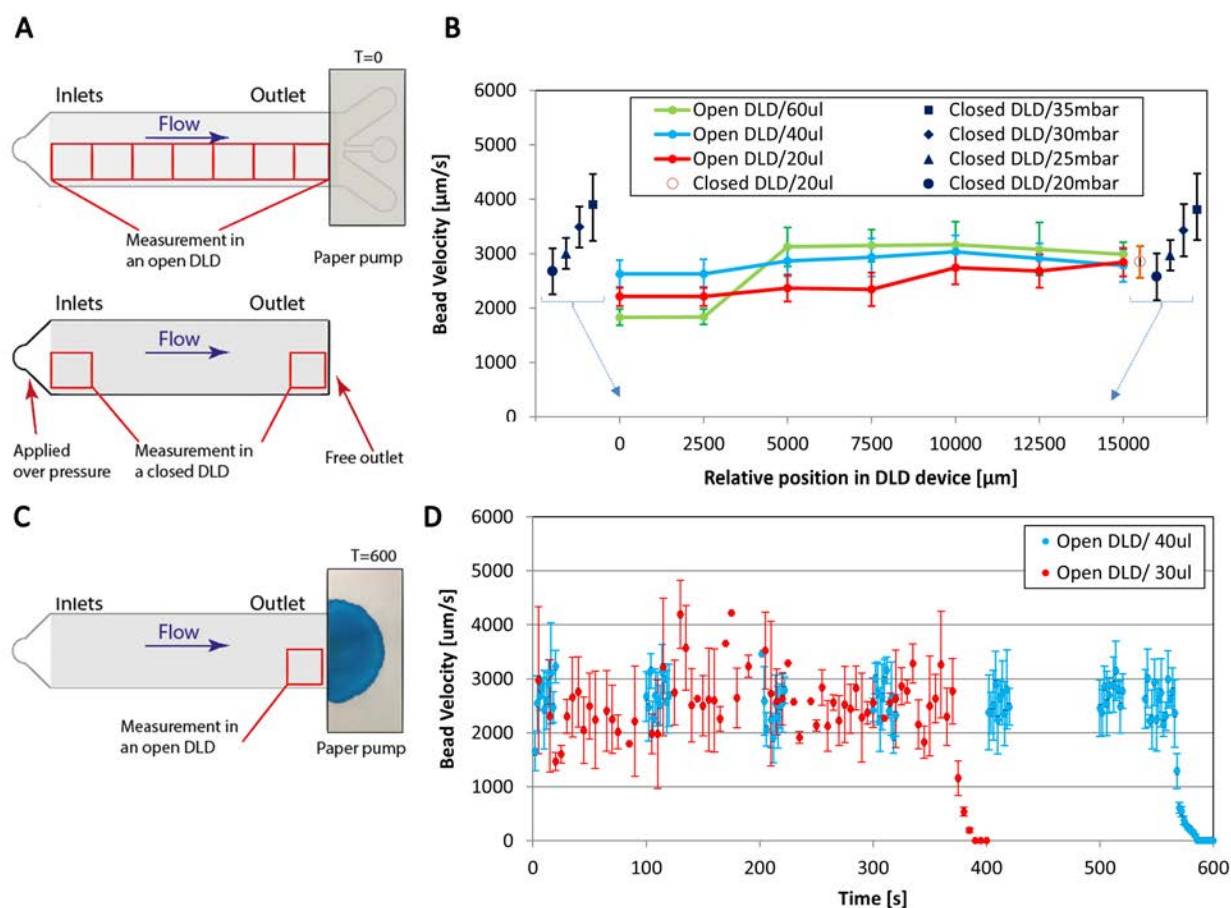


Figure S4. Particle velocity measurements for open and closed DLD devices. The flow in the open devices is driven by a paper capillary pump without any wax-defined channels. The paper is shown at $t=0$ s in (A) and $t=600$ s in (C). The flow in the closed devices is driven by over pressure as well as by a paper capillary pump. The different sets of experiments took place using the same design of DLD (Device 1 (Figure S1)). The following microspheres were used at a dilution of 50x in deionized water: green fluorescent polystyrene beads with diameter $1.57 \mu\text{m}$ (CV 2%) and functionalized with carboxylate groups from Polysciences Inc. (Warrington, PA). (A) Schematic of measurement setup for velocity measurements at different locations for open and closed devices. (B) Velocity of the beads as a function of position for open and closed devices. For the data where a paper capillary pump was used the volume in the reservoir is indicated. For the pressure driven flow the applied pressure difference is given. (C) Schematic of measurement setup for velocity measurements as a function of time. (D) Velocity of beads as a function of time when 30 μL (red) and 40 μL (blue) of sample is added to the reservoir. The error bars represent the standard deviations of the measurements.

For the images with the macro objective, the device is wetted with an aqueous food dye and imaged, with the liquid facing upwards, using a macro objective (Canon MP-E 65 mm f/2.8 1-5x) with a Canon 5D Mark II camera house. Basic contrast and brightness adjustments were made to ensure that the image reflects what is seen by the naked eye.

We could observe a tendency that the flow velocity (see below) is slightly lower for the first ~5 mm along the device. This indicates that the flow cross section is larger here, which is consistent with the flow extending above the posts since the volume flow rate is a conserved quantity. We observed that this effect vanishes as the fluid level drops, away from the reservoir and also decreases as the sample volume in the reservoir decreases with time.

Flow measurements

We measured the flow rates at different positions along open and closed devices using an applied overpressure or using a paper capillary pump (Figure S4). Velocities of fluorescent microspheres were observed between two neighboring posts in the same row.

The volumetric flow rates were measured directly by running the device with reservoirs filled with well-defined volumes and recording the elapsed time until the reservoirs were empty (Figure S4D). The volumes were corrected by subtracting the evaporated volume from the device based on figure S5 (8.5 nL/s). The time was measured until the velocity was half of the mean velocity. The remaining liquid in the device was crudely estimated to half the volume of the device, i.e. $0.5 \times 1.1 \mu\text{L}$. This volume was subtracted from the total volume considered. From these two measurements we obtain approximate values of 70 nL/s and 61 nL/s for the two different volumes tested. These results are consistent with the results of combining the velocity measurements (Figure S4B) with the total flow cross section based on the designed dimensions (Device 1 in Figure S1C) of the device giving flow rates of 71 ± 19 nL/s. The correspondence of the two types of measurements indicate that the flow is indeed taking place such that it fills up the space between the posts without overflowing.

Equivalent pressures applied to the device

The equivalent pressure exerted by the paper capillary pump is found to be 21 mBar by comparing the applied over-pressure necessary across a closed device to achieve the same flow velocities as for a closed device with a paper capillary pump (Figure S4B). The pressure exerted by the paper capillary pump exceeds the pressure due to the water pillar in the reservoir. The pressure generated in the reservoir depends on the height difference between the inlet and outlet ($\rho g \Delta h \sim 1$ mBar/cm with $\rho = 1000$ kg/m³ density of water, $g = 9.8$ m/s² gravitational acceleration, Δh height of water pillar). The tested volumes, 30 μL , 40 μL and 60 μL , correspond to heights of 4.2 mm, 5.6 mm and 8.4 mm of sample respectively in the reservoir (inner diameter 3mm) giving hydrostatic pressures of 0.4 mBar, 0.6 mBar and 0.8 mBar which is much less than the involved estimated negative pressures exerted by the capillary paper pump pulling the sample. The capillary pumping effect of the paper therefore dominates the flow and the fluid is predominantly pulled through the device.

Flow resistance

Flow resistance for the closed devices is estimated based on the relationship

$$Q_{pump}^{closed} = \frac{\Delta P_{pump}}{R_{load}^{closed}}$$

where R is the fluidic resistance, Q is the volumetric flow rate and ΔP is the applied pressure difference across the device. From figure S4B we obtain $R^{closed} = 30 \cdot 10^{12} \text{ kgs}^{-1} \text{ m}^{-4}$.

The flow resistance of the open device is expected to be slightly lower than that for the closed device. It is calculated below based on figure S5.

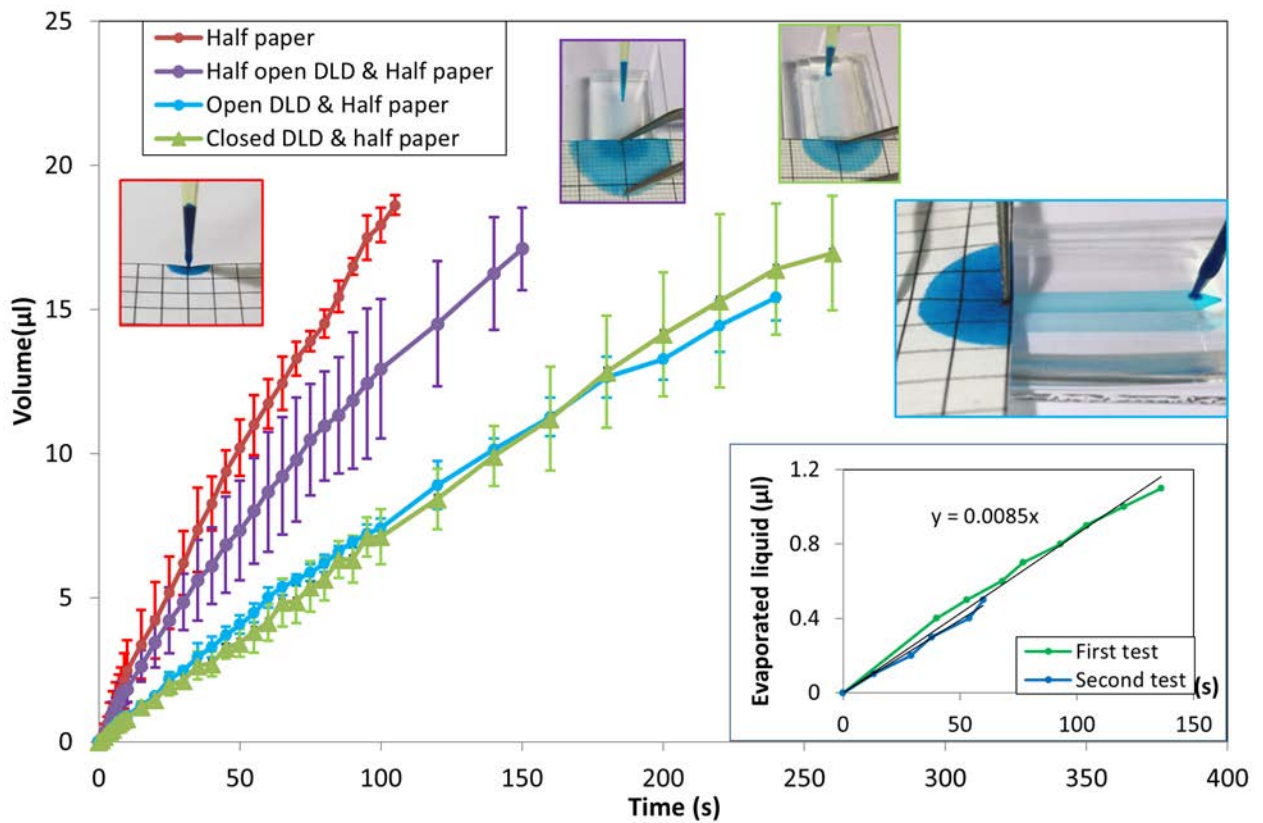


Figure S5. Liquid flows versus time corrected for evaporation. The liquid is 0.5% food coloring diluted in deionized water. The graph shows four cases. From the left to the right we have: liquid added at the edge of a paper (half paper), open DLD device of length 10 mm (half device) connected to paper, open DLD of length 20 mm (whole device) connected to paper, closed DLD of length 20 mm (whole device) connected to paper. To be able to easily judge the extent of the drops on the paper, a grid pattern is printed on the paper using a standard laser writer. The inset shows the accumulated evaporated liquid from a filled device (device 1). From this graph we can conclude that the evaporation rate from the device is 8.5 nL per second.

Characterization of the paper capillary pump

The paper capillary pump can be treated as a battery with an internal resistance and an internal negative pressure or, in analogy to electronics, a hydromotive force. To estimate the internal resistance and the hydromotive force the following system of equations (number 1 to 4) are considered. Note that we will obtain an estimate of the flow resistance of the open device from these calculations.

$$\left\{ \begin{array}{l} Q_{paper} = \frac{\Delta P_{internal}}{R_{internal}} \\ Q_{paper}^{openHALF} = \frac{\Delta P_{internal}}{\frac{1}{2}R_{load}^{open} + R_{internal}} \\ Q_{paper}^{open} = \frac{\Delta P_{internal}}{R_{load}^{open} + R_{internal}} \\ Q_{paper}^{closed} = \frac{\Delta P_{internal}}{R_{load}^{closed} + R_{internal}} \end{array} \right.$$

We first calculate the internal resistance of the paper by combining equations 1 and 4 above to eliminate the internal pressure (hydromotive force).

$$R_{internal} = \frac{\Delta P_{pump}}{Q_{pump}^{closed}} \frac{Q_{paper}^{closed}}{Q_{paper}^{closed} - Q_{pump}^{closed}}$$

Numerical data is extracted from Figures S4 (for the pump driven flow) and S5 (for the paper capillary pump driven flow) based on the initial flow rates for each case and combined with the flow resistance of the closed device as calculated above.

$$\begin{aligned} \Delta P_{pump} &= 21 \text{ mBar} \\ Q_{pump}^{closed} &= 71 \text{ nLs}^{-1} \\ Q_{paper} &= 198 \text{ nLs}^{-1} \\ Q_{paper}^{closed} &= 71 \text{ nLs}^{-1} \\ \Rightarrow R_{internal} &= 16.5 \cdot 10^{12} \text{ kg s}^{-1} \text{ m}^{-4} \end{aligned}$$

The hydromotive force is now calculated by using the number of the flow rate of the paper without any device ("Half paper") in fig S5 combined with equation 1 above.

$$\begin{aligned} Q_{paper} &= 198 \text{ nLs}^{-1} \\ \Rightarrow \Delta P_{internal} &= 32 \text{ mBar} \end{aligned}$$

Plugging the results above into equation 3 above, the flow resistance of the open device.

$$\begin{aligned} Q_{paper}^{open} &= 80 \text{ nLs}^{-1} \\ \Rightarrow R_{load}^{open} &= 23.1 \cdot 10^{12} \text{ kg s}^{-1} \text{ m}^{-4} \end{aligned}$$

Finally, as a simple control the flow rate of the device cut in half is estimated based on equation 2 above.

$$Q_{paper}^{openHALF*} = 113 nLs^{-1}$$

The value is lower but still consistent with the value obtained by measuring the initial slope of the corresponding curve in figure S5.

$$Q_{paper}^{openHALF} = 157 nLs^{-1}$$

Evaporation

To obtain rough estimates of the evaporation rates we measured the evaporation rates for different cases by using a precision balance (Ohaus Corp. Pine Brook, NJ USA, model Pioneer PA114C, minimal readout 1 μ g).

An evaporation of 8 nL/s from the device can be compared to the typical flow rate through the device of 65 nL/s. Roughly 12% of the sample is thus evaporated from the device.

Due to nonuniform wetting and possible variations in the lab environment during the course of the experiments, the evaporation rates should be considered rough estimates to give a perspective of the relationship between the evaporation rate and the volumetric throughput in the devices.

The lab environment had a $60 \pm 5\%$ RH and room temperature of $21^\circ \pm 1^\circ$ C.

Biological samples

The size distributions of the biological samples used were determined by measurement in optical micrographs using ImageJ (Figure S6). The results are summarized in the following table.

<i>Sample type</i>	<i>Dimensions \pm std dev</i>	<i>Shape</i>
MCF7 (cancer cell line)	$17.3 \pm 2.1 \mu\text{m}$	spherical
White blood cell	$12.2 \pm 0.9 \mu\text{m}$	spherical
Red blood cell	$2.2 \pm 0.5 \mu\text{m}$ $7.8 \pm 0.6 \mu\text{m}$	biconcave
<i>Trypanosome cyclops</i>	$2.5 \pm 0.5 \mu\text{m}$ $12.8 \pm 3.3 \mu\text{m}$	ribbon-like

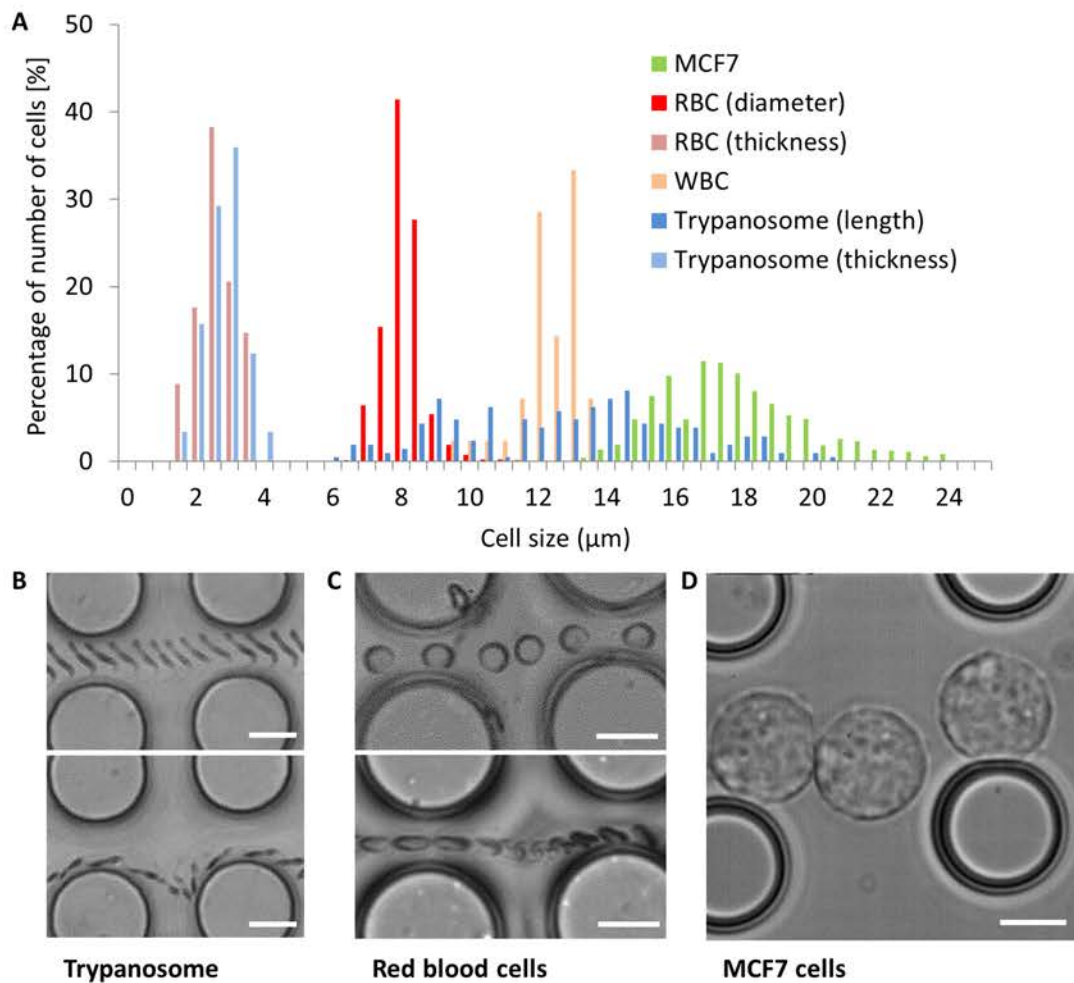


Figure S6. Size distribution of biological samples based on measurements in optical micrographs. (A) Histograms of size distributions. For the spherical cells (MCF7 and WBC) one number gives the relevant size (diameter). Red blood cells and the parasites are described by two numbers (thickness and overall diameter or length). (B) & (C) Optical micrographs of the non-spherical cells exhibiting different orientations depending on device depth ($9\ \mu\text{m}$ and $24\ \mu\text{m}$) (top images shallow device and bottom images deep device) (D) Optical micrograph of spherical MCF7 cells. All scale bars $10\ \mu\text{m}$.

Manuscript

Softness Sorting for Cancer Cells

Softness sorting for cancer cell

T. S. H. Tran^a, J. P. Beech^b and J. O. Tegenfeldt

Due to their direct association with the physiology of cancer cells, physical properties are especially attractive as markers for sorting and characterization. Where molecular surface markers are lacking, the physical properties can instead serve as inherent markers for separation. Indications that soft cancer cells are more metastatic than hard cells make mechanical properties of specific interest. Our work provides a deeper understanding of deformability based sorting based on deterministic lateral displacement (DLD) and will be used to optimize DLD devices for the characterization and fractionation of cancer cells into subpopulations with different mechanical properties. Our aim is to develop a device to help oncologists gain more accurate prognoses and better monitoring of the effect of treatment.

Introduction

During the last decade, the deterministic lateral displacement technique has been developed and applied to an increasing variety of biological samples. Since the first application for particle and DNA separation (1), significant advances have been reported which improve our understanding of the theory as well as design considerations for new and challenging samples. Examples of DLD applications are the fractionation of blood components (2-5), isolation of cancer cells from blood cells (6-8), parasite separation (9, 10) and the isolation of extracellular vesicles (11-13).

Essentially, deterministic lateral displacement is a size-based sorting technique. By precisely controlling the geometry of obstacle arrays, DLD has been shown to be a powerful sorting technique with high-resolution (12) and throughput (14). In 2011, Holm *et al.* first reported the use of the method as a morphology-based sorting tool when they extracted parasites from blood (9) and in 2012, Beech *et al.* further extended the method to deformability-based sorting of red blood cells (15) and platelets (16). These capabilities make DLD very interesting for label free cell sorting and analysis.

In a DLD device, an array of posts is designed with different parameters: gap size, post size and post shape as well as critical radius, R_c , which is selected depending on the intended targets. For hard polystyrene spherical particles, particles smaller than a critical size move along the flow while the particles larger than the critical size displace and switch to neighboring streamline (Fig 1A and B). However,

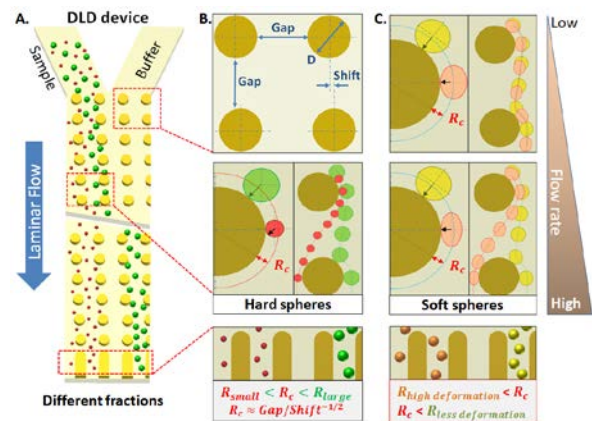


Figure 1. Schematic overview of deformability-based separation in a DLD device. (A.) A cartoon depiction of a DLD device in which a mixture of particles (large green and small red particles) and buffer are loaded in the inlet. Particle trajectories, which show a separation of displaced (green) and non-displaced (red) particles, illustrate the basic operation of DLD. (B.) Several parameters determine the performance of a DLD device. Of these, the critical size (R_c) is the primary decider of how the device can discriminate small and large particles. Particles larger than the critical size are “displaced” while smaller ones follow the flow direction in “zigzag” mode. As a result, particles exit the device at different outlets. (C.) In the case of soft particles and high shear forces, the deformability changes the particle effective size and changes the distribution of particles at the outlets. Orange particles, which are the same size as the yellow particles but softer, are shifted to the zigzag mode and separated from the more rigid particles.

for biological applications, the samples often are soft and deformable, such that the flow rate affects their trajectories as shown in Figure 1C.

Due to shear forces generated in the device, the soft particle seems to be smaller at high flow rates than at low

flow rates. When the effective size of particles is smaller than the designed critical size of the array, the large particles change from the displacement mode to zigzag mode. By carefully evaluating the correlation of deformed radius and flow rate, we can characterize the deformability of each cell type and then re-design the DLD geometry to achieve a deformability-based separation.

Our targeted cells in this work are MCF7 (human breast cancer cell line) and MCF10A (human breast cell line), which are still considered challenging to sort due to the similarity of physical properties (shape and size) and instead currently are distinguished by labelling with specific antibodies.

Result and discussion

Soft particles in DLD

Polystyrene and polyacrylamide particles (both diameter $15\mu\text{m}$, and Young's modulus of $3\text{-}3.6\times 10^9\text{Pa}$ and $4\text{-}9.5\times 10^2\text{Pa}$) are used as a reference for the calibration process. While the rigid particles (polystyrene) are unaffected when increasing flow rate, the soft particles (polyacrylamide) are expected to deform and therefore be less displaced at higher shear rates. Figure 2A shows two frames from a movie where a soft, polyacrylamide, particle (transparent and non-fluorescent) can be seen interacting with an obstacle (300mbar). Deformation cannot be seen in these images. Fig. 2B shows the average trajectories of ten polyacrylamide particles at three pressures. Because the particle size is larger than the critical size ($D_c=14\mu\text{m}$), all particles are displaced in the array at 300mbar. A transition takes place at 500mbar where particles appear both in the zigzag and displacement mode. At 700mbar, the transition is completed and all particles behave as if they were smaller than the critical size. We believe that this is primarily due to deformation of the particles in the shear flow and in interactions with the posts.

The distribution of the soft polyacrylamide particles at the end of a device as a function of the applied pressure is shown in Fig 2C. Particles smaller than the critical size are collected in the zigzag area. We can clearly see how the distribution moves to the left (less displacement) as the pressure is increased. The data illustrates a capability of softness sorting in DLD for soft particles.

Cell Characteristics

Cell size and morphology are commonly used as label-free markers to distinguish different cell types. This is particularly difficult for some cancer cells however due to their similarities in size and shape to the corresponding

normal cells. Cancer cells are reported to have wide-ranging sizes and irregular shapes that overlap with the distributions of the corresponding non-cancerous cells. In this study we use two cell lines, MCF10A, a non-cancerous human breast cell line and MCF7, a cancerous human breast cell line. We use DLD to explore differences in the mechanical properties of these otherwise similar cells.

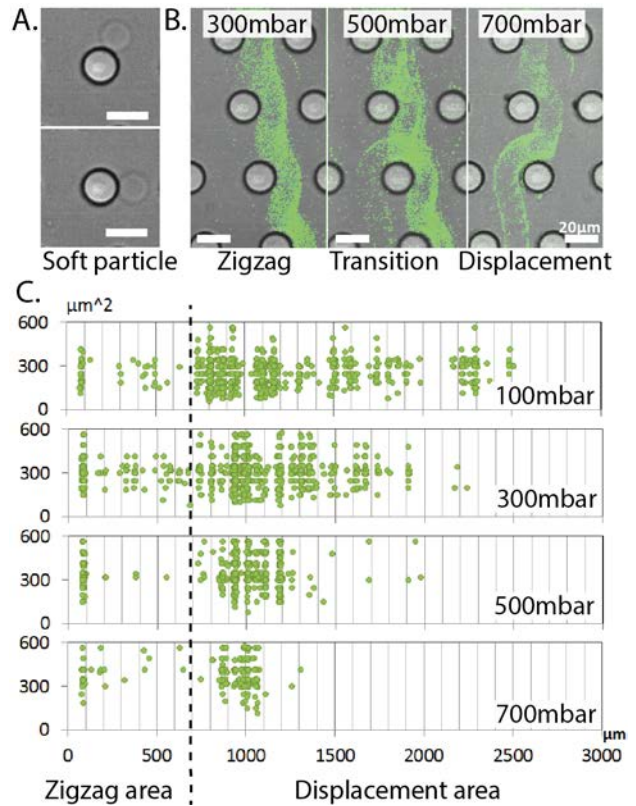


Figure 2. Soft hydrogel particles in DLD array. (A.) Consecutive images of a soft and transparent particle interacting with a post. (B.) Time averages of many particle traces of the same kind of particle (polyacrylamide) as shown in A. Transition from displacement mode to zigzag mode occurs as the pressure is increased. (C.) Particle distributions at the end of the separation array. Particles become effectively smaller (less displaced) as the pressure is increased.

The size and shape of MCF7 and MCF10A cells was determined by optical microscopy of a suspended mixture of the two cell types (Fig 3). Our MCF7 cells express GFP and were identified using fluorescence (red arrows). The two cell types were classified into three groups (single cells, double cells and aggregates (three cells or more) and the cell area and circularity measured. Fig 3C shows cell area and circularity for a population of MCF7 cells after trypsinization to release them from culture flasks. Some rare aggregates were as large as $10\,000\ \mu\text{m}^2$ but for

clarity the plot is limited to the range 0 to 3000 μm^2 . Due to the spherical shape of suspended cells, a circularity number can be used to represent cell shape or morphology.

Cell aggregation is a significant practical challenge for single cell analysis. Cancer cells that divide uncontrollably form aggregates or clusters more easily than normal cells (12% of cells in aggregates for MCF7 and only 3% for MCF10A for the present study). In microfluidics devices, cell aggregates are a common cause of clogging. To prevent clogging in the DLD array, an upstream filter array is integrated into the device, which captures aggregates. Single cells are able to pass the filter and are guided to the main DLD array for evaluation of deformation and for sorting.

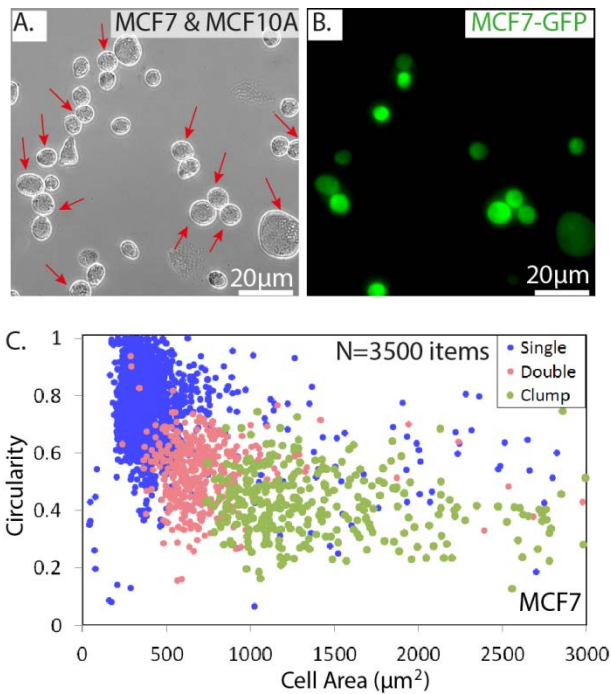


Figure 3. Microscopic inspection and analysis of MCF7 and MCF10A for size, shape and aggregation. (A.) A bright-field image provides an overview of MCF7 and MCF10A cells, which are similar in size and morphology. (B.) Fluorescence image of MCF7 (labelled with GFP) is used to identify MCF7 cells in the mixture. (C.) The size (cell area), shape (circularity) and level of aggregation (single, double or aggregates of 3 or more) was determined. The graph provides the data of MCF7 cells.

The size distributions of MCF7 and MCF10 cells are presented in Figure 4. The cells have the same average size ($D=19\mu\text{m}$) and shape (close to round with $C=0.8$). However, the variance in size and shape of the cancer cells is somewhat wider than for the normal cells (table in Fig.4) as is expected from the literature (17). To summarize, suspended MCF7 cells easily form aggregates (12%) and they have a wider distribution in size ($D=19\pm 4\mu\text{m}$) with uniform shape ($C=0.76\pm 0.12$) while MCF10A are more uniform in size and shape ($D=19\pm 2\mu\text{m}$ and $C=0.4-1$) and show less aggregation (3%).

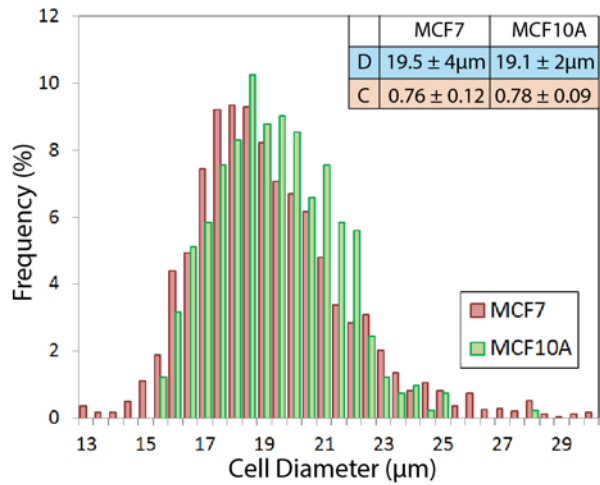


Figure 4. Cell diameter distribution of both MCF7 and MCF10A cells. The table presents the average value and variance of diameters (D) and circularities (C).

Cell behaviour at different flow rates

Based on our results with hard and soft particles we expect the softer cancer cells to deform more readily at higher flow rates in our DLD devices. Using a high-speed camera with high frame rates ($\sim 10\,000$ fps), we were able to capture and analyze the behaviour of individual cells as they flow through our devices. Fig. 5A clearly shows that a single MCF7 cell deforms when interacting with a post. Furthermore, the trajectories of small and large cells illustrate the sorting mechanism of DLD array at low shear stress and a difference of large cells when moving at a higher shear rate (Fig. 5B).

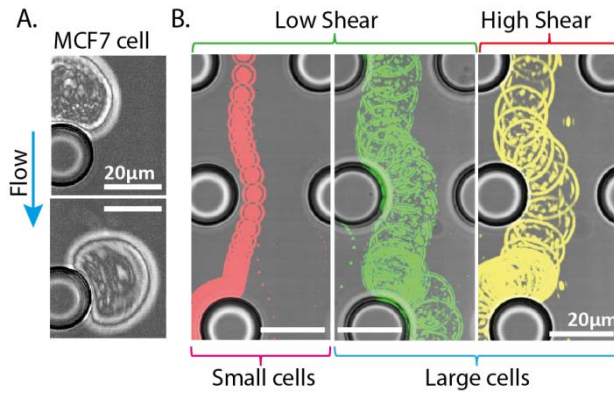


Figure 5. Cell trajectories due to different size and deformation effects. (A.) A single MCF7 cell is deformed when interacting with a post (B.) In the low shear, cell performance follows the expected paths (small ones are in zigzag mode while large ones are displaced). When increasing the shear rate, large cells start deforming and the effective size is decreased such that the trajectory is greatly affected. When the effective size is smaller than the critical size, large cells move along a zigzag path.

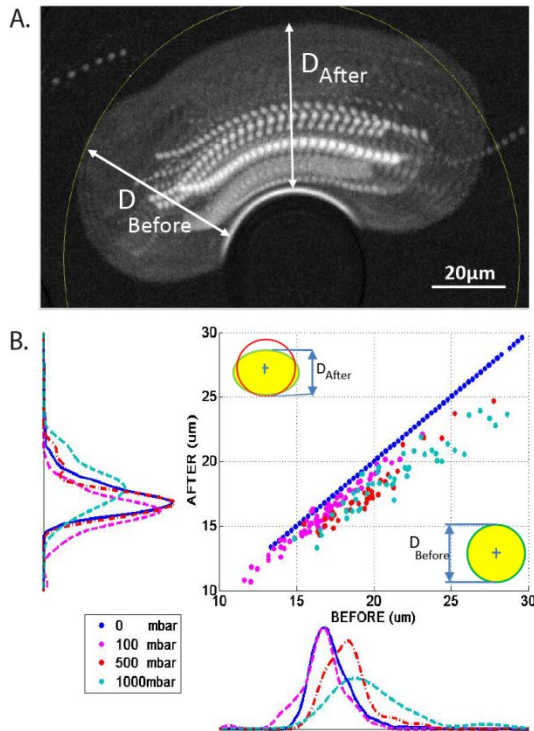


Figure 6. Individual cell deformations due to contact with a DLD post. (A.) Cell tracking image before and during interacting with a post. (B.) The correlation between cell diameter before and during contact with a post. Deformation due to interaction with the post is greater for higher pressures.

A measurement of cell deformation rate is conducted based on the cell diameter before and during contact with the post. The data is plotted in Fig. 6B. Note the blue dotted line that serves as a reference for the measurement at 0 mbar (no flow and therefore no deformation).

A difference in effective size was observed as a function of flow rate. Applied pressures of 100, 500 and 1000mbar caused measured deformations of 2, 8 and 17%. Bigger cells (>20μm) seem to deform to a greater extent than small ones (<20μm) in all cases. Data were collected for MCF7 cells only.

Cell separation based on deformability

Since the aim in this study was to separate cancer cells from normal cells based on deformability, the distributions of both kinds of cells were characterized carefully at a variety of applied pressures. Cells were imaged and counted at the outlet of the device. The distribution of cells was plotted as a function of applied pressure. Each cell's position at the end of the array indicates its effective size, which is the size of a non-deformable particle that arrives at the same position.

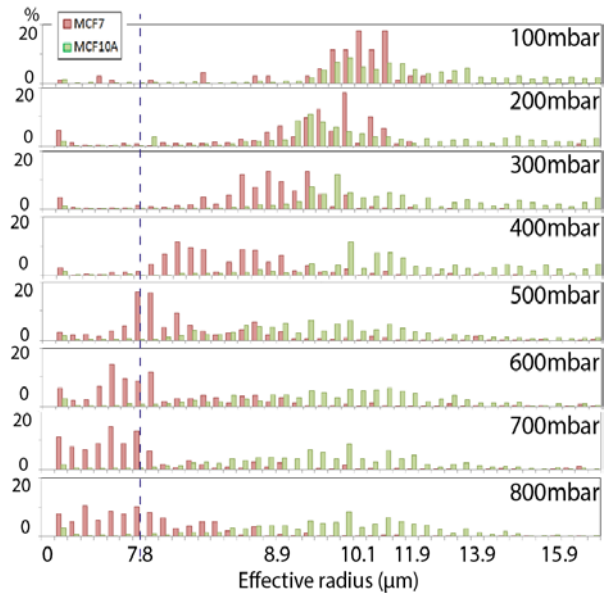


Figure 7. Outlet distribution of MCF7 and MC10A cells when increasing the applied pressures (from 100mbar to 800mbar). Data were collected from separate experiments of MCF7 and MCF10A cells.

We observed that MCF7 cells are softer than MCF10A cells. At low flow rates (low pressure at 100mbar), the two distributions overlap and no sorting occurs. When the flow rate gradually increases, MCF7 cells start shifting to the left, meaning that their effective sizes

decrease more rapidly than for MCF10 cells. At 700mbar the separation is significant. At 800mbar, the distribution of MCF7 cells slightly returns to the right side. This might be due to the limit of the designed critical size in the DLD array (smallest value is 7.8 μ m).

Overall, the data provide a strong correlation of cell deformation and the flow rate in MCF7 cells. It also supports a capability of sorting those cells based on deformability.

Materials and Methods

Device fabrication

In a contact mask aligner (Karl Suss MJB3 and MJB4, Munich, Germany), negative photoresist SU8 (MicroChem, Newton, MA, USA) spun on a 3" silicon wafer was exposed to UV light through a chrome-mask designed in L-Edit 11.02 (Tanner Research, Monrovia, CA USA) and printed by Delta Mask (Delta Mask, Enschede, The Netherlands). Before casting of PDMS, a monolayer of 1H,1H,2H,2H-perfluorooctyltrichlorosilane (ABC R GmbH & Co. KG, Karlsruhe, Germany) was applied to the master as an anti-adhesion agent to facilitate demolding. A 10:1 mixture (monomer: curing agent) of PDMS (Sylgard 184, Dow Corning, Midland, MI, USA) was degassed, poured onto the master then baked for 2 hours at 80°C.

To bond the device to glass, the PDMS device and the glass were treated with oxygen plasma (Plasmatic Systems, Inc., North Brunswick, NJ, USA). Subsequently, holes were punched at the inlets and outlets and silicon reservoirs were glued.

Sample preparation

Fluorescently labeled polystyrene microspheres with a diameter of 15 μ m and 20 μ m from Polyscience Inc., Warrington, PA, USA were suspended in milliQ water and used in varying flow rate for calibration.

MCF-7 and MCF-10A (breast carcinoma cell lines and human breast epithelial cell lines obtained from the American Type Culture Collection (ATCC)) were cultured at 37°C and 5% CO₂. Cell culture medium for MCF-7 was DMEM, 10%FBS and 1% Penicillin-Streptomycin (Sigma-Aldrich). And cell culture medium for MCF-10A was DMEM, 5% Horse Serum, 20ng/ml Epidermal Growth Factor (EGF), 10ug/mL Insulin, 0.5ug/mL Hydrocortisone, 100ng/mL Cholera Toxin and 1% Penicillin-Streptomycin (Sigma-Aldrich). After a one-week subculture, the cells proliferated to fill more than 85-90% of the surface of the culture flasks and were considered ready for separation experiments.

Image acquisition and analysis

Particle and cell distributions were calculated from images acquired using an inverted epifluorescence microscope (Nikon Eclipse Ti, Nikon Corporation, Tokyo, Japan) and scientific CMOS camera (Flash4.0 V2, Hamamatsu, Japan) and an EoSens mini MC-1370 fast camera (Mikrotron GmbH, Unterschleissheim, Germany) for high frame rate imaging. ImageJ software, downloaded from the National Institutes of Health, was used for image analysis and the preparation of figures. Code written using Matlab R2014a was used for image analysis tailored to the specific needs of cell counting and morphology detection.

All error bars of data shown in graphs and figures represent \pm one standard deviation.

Conclusions

We have successfully demonstrated and measured the deformability of breast cells (MCF10A) and breast cancer cells (MCF7) using DLD devices. We find that the MCF7 cells are deformed more than 10% at the highest flow rates used. We show successful proof of principle of complete separation of MCF7 cells from the relatively much harder non-malignant cell type MCF10A.

Acknowledgements

We thank Bo Baldetorp for his donation of MCF-7 and MCF-10A cells. This work was carried out within NanoLund at Lund University with funding from the Child Cancer Foundation (MT2013-0031), LAPASO (EU FP7 project 607350) and the Swedish Research Council (VR) grant no. 2015-05426. All device processing was conducted within Lund Nano Lab.

References

1. Huang LR, Cox EC, Austin RH, & Sturm JC (2004) Continuous particle separation through deterministic lateral displacement. *Science* 304(5673):987-990.
2. Inglis DW, Lord M, & Nordon RE (2011) Scaling deterministic lateral displacement arrays for high throughput and dilution-free enrichment of leukocytes. *Journal of Micromechanics and Microengineering* 21(5):054024.
3. Civin CI, *et al.* (2016) Automated leukocyte processing by microfluidic deterministic lateral displacement. *Cytometry. Part A : the journal of*

- the International Society for Analytical Cytology* 89(12):1073-1083.
4. Zeming KK, Salafi T, Chen CH, & Zhang Y (2016) Asymmetrical Deterministic Lateral Displacement Gaps for Dual Functions of Enhanced Separation and Throughput of Red Blood Cells. *Scientific reports* 6:22934.
 5. Yamada M, Seko W, Yanai T, Ninomiya K, & Seki M (2017) Slanted, asymmetric microfluidic lattices as size-selective sieves for continuous particle/cell sorting. *Lab on a chip* 17(2):304-314.
 6. Louterback K, *et al.* (2012) Deterministic separation of cancer cells from blood at 10 mL/min. *AIP Adv* 2(4):42107.
 7. Liu Z, *et al.* (2013) Rapid isolation of cancer cells using microfluidic deterministic lateral displacement structure. *Biomicrofluidics* 7(1):11801.
 8. Okano H, *et al.* (2015) Enrichment of circulating tumor cells in tumor-bearing mouse blood by a deterministic lateral displacement microfluidic device. *Biomedical microdevices* 17(3):9964.
 9. Holm SH, Beech JP, Barrett MP, & Tegenfeldt JO (2011) Separation of parasites from human blood using deterministic lateral displacement. *Lab on a chip* 11(7):1326-1332.
 10. Holm SH, Beech JP, Barrett MP, & Tegenfeldt JO (2016) Simplifying microfluidic separation devices towards field-detection of blood parasites. *Anal Methods-Uk* 8(16):3291-3300.
 11. Santana SM, Antonyak MA, Cerione RA, & Kirby BJ (2014) Microfluidic isolation of cancer-cell-derived microvesicles from heterogeneous extracellular shed vesicle populations. *Biomedical microdevices* 16(6):869-877.
 12. Wunsch BH, *et al.* (2016) Nanoscale lateral displacement arrays for the separation of exosomes and colloids down to 20 nm. *Nature nanotechnology* 11(11):936-940.
 13. Pariset E, Agache V, & Millet A (2017) Extracellular Vesicles: Isolation Methods. *Advanced Biosystems* 1(5):1700040.
 14. Louterback K, *et al.* (2012) Deterministic separation of cancer cells from blood at 10 mL/min. *Aip Adv* 2(4).
 15. Beech JP, Holm SH, Adolfsson K, & Tegenfeldt JO (2012) Sorting cells by size, shape and deformability. *Lab on a chip* 12(6):1048-1051.
 16. Henry E, *et al.* (2016) Sorting cells by their dynamical properties. *Scientific reports* 6:34375.
 17. Hanahan D & Weinberg RA (2000) The Hallmarks of Cancer. *Cell* 100(1):57-70.

